Closed-loop recycling of Li-ion batteries

An integration between hydrometallurgy and bipolar membrane electrodialysis

Filip van Efferink

Closed-loop recycling of Li-ion batteries

An integration between hydrometallurgy and bipolar membrane electrodialysis

by

Filip van Efferink

In Fulfillment of the Requirements for the Degree of
Energy, Flow and Process Technology

Student number:	4662830
Supervisor:	Dr. M. Ramdin
Starting month:	January 2024
Faculty:	Mechanical Engineering

TU Delft

To my first science teacher, grandfather Anatoli

Abstract

The percentage of electric vehicles (EVs) in the automotive sector is expected to quadruple by 2040, causing concern regarding the material supply required for the production of lithium-ion batteries. Currently, a substantial part of these materials, such as cobalt and lithium, are subject to non-circular economies, have a substantial environmental impact and are mined in countries with unstable political situations.

Up until now, numerous companies have attempted to resolve these issues through the use of pyro- and hydrometallurgical recycling methods. However, they are yet to meet the mandated recycling goals put in place by the European Commision. This enhances the urgency for the development of a novel, efficient and scalable technology for the recovery of valuable material from spent lithium-ion batteries.

In order to achieve such a development, this study proposes to incorporate Bipolar Membrane Electrodialysis into the standard hydrometallurgical recycling approach. During the course of this research, a prototype of this technology was realized and used to investigate its effectiveness. For practical reasons, the research focused exclusively on the metal and acid recovery from leached LCO cathode material.

Within the subsequent experimental phase of this research a critical issue was identified. Namely, the tendency of divalent cobalt ions to precipitate in non-acidic media. The resolution to this issue required the incorporation of Donnan dialysis into the built BPMED setup, which was used to adjust the acidity of the solutions within the different electrolytic compartments.

Ultimately, this approach led to the respectively recovery of 14 and 22 percent of the lithium and cobalt initially present in the feed solution. Simultaneously, the study recovered a significant amount of the starting leaching agent in the form of 0.6 M nitric acid. Whilst additional optimizations are required to improve the recovery efficiencies, the study successfully demonstrates a proof of concept of the proposed solution.

Contents

List of Figures

List of Tables

Nomenclature

Abbreviations

Abbreviation	Definition
AEM	Anion Exchange Membrane
Bo	Bond number
BPMED	Bipolar Membrane Electrodialysis
BPM	Bipolar Exchange Membrane
CEM	Cation Exchange Membrane
ED	Electrodialysis
EV	Electric Vehicle
IC	Ion-Chromatograph
ICP	Inductively Coupled Plasma
LCO	Lithium Cobalt Oxide
LIB	Lithium Ion Battery
LFP	Lithium Iron Phosphate
LMO	Lithium Manganese Oxide
NCA	Nickel Cobalt Aluminium
NCM	Nickel Cobalt Manganese
PVDF	Polyvinylidene Fluoride
XRD	X-ray Diffraction

1 Introduction

1.1. The lithium-ion battery: development and prospects

Originally commercialized by Sony towards the end of the 20th century, the lithium-ion battery (LIB) has since become an unmissable component in a huge variety of technological appliances [1, 2]. Demand for this technology, currently at an all-time high, has increased exponentially over the past couple of decades and is projected to continue its rapid growth far into the future. Two main factors influencing this trend are the rapid increase in global vehicle (EV) production and the urgent call for more efficient energy storage solutions. To put things into perspective, in 2022 EVs comprised a fraction of 14 % of all car sales worldwide. By as early as 2040, however, this fraction could increase to a value of 58 % [3]. Furthermore, the demand for LIBs can be explained from a technological standpoint. LIBs are known to have a high voltage and energy density, long-life cycle and low self-discharge [2, 4, 5]. Factors, that make the potential development of a competitive alternative unlikely. Nevertheless, apart from the numerous advantages that LIBs hold over other energy storage solutions, LIBs suffer from a number of inherent environmental, political and financial drawbacks.

For starters, LIBs aren't easily recyclable. In fact, without an immediate and scalable improvement in recycling technology, debris generated from LIBs use could grow to as much as 800 million tonnes by 2050. Meanwhile, the debris that LIBs produce is toxic in nature, which could potentially lead to, in addition to other things, the production of toxic gases. Furthermore, a majority of the lithium and cobalt used in LIBs are produced from primary resources, which typically involve energy intensive and water demanding steps. Lithium, for example, is either extracted and leached from ores/minerals such as Spodumene, or obtained through a series of chemical processes from brines [6]. In some places, such as Salar de Atacama in Chile, the latter process has already led to significant water depletion [7]. As water scarcity is often prevalent in places where brines are located, unsustainable fresh and saltwater management can put significant pressure on local populations and ecosystems. Cobalt, on the other hand, is produced as a by-product of either nickel or copper production and leads to a carbon footprint similar to that of lithium, around $\times\ 10^6$ kg of carbon dioxide equivalent [8, 9].

As for the political argument it's worth mentioning that expensive metal material that is incorporated into the cathode structures of LIBs are often mined in countries with unstable political situations, raising concern surrounding the stability of the metal supply. To put things into perspective, 59 % of the global Cobalt production originates from the African Copperbelt, situated largely inside the Democratic Republic of Congo (DRC) [10]. Whilst The United Nations peacekeeping mission in the Democratic Republic of the Congo (MONUSCO) is currently undergoing withdrawal from the DRC, the United Nations Security Council nonetheless notes that the "DRC continues to suffer from recurring and evolving cycles of conflict and persistent violence by foreign and domestic armed groups" [11]. Meaning that the region remains prone to escalation, which could potentially lead to disruptions in the metal supply chain.

From the economic argument, it is important to note that metal rich cathode material is typically the most expensive component of a Li-ion battery, amounting to an estimated 70 % of the total battery cost

[12]. On top of that, Lithium-ion batteries are costly themselves, ranging up to half of the total price of an EV. Therefore, any additional expenditures aimed at increasing the circularity of the metal material may significantly increase the overall cost of an EV, hindering the development of recycling technology.

All things considered, the total of environmental, political and economic issues associated with the immense popularity of the LIB technology raise a cause for concern. Immediate improvements for the circularity of the most critical components are therefore required and act as the main motivator behind the research conducted in this report.

1.2. Common recycling solution

In order to motivate advancements in battery recycling techniques necessary to combat the current non-circularity of LIBs, the European Commission has set a number of quantifiable targets [13]. Some relevant fragments of these targets, such as the desired future recovery rates for lithium and cobalt, are summarized in figure 1.1.

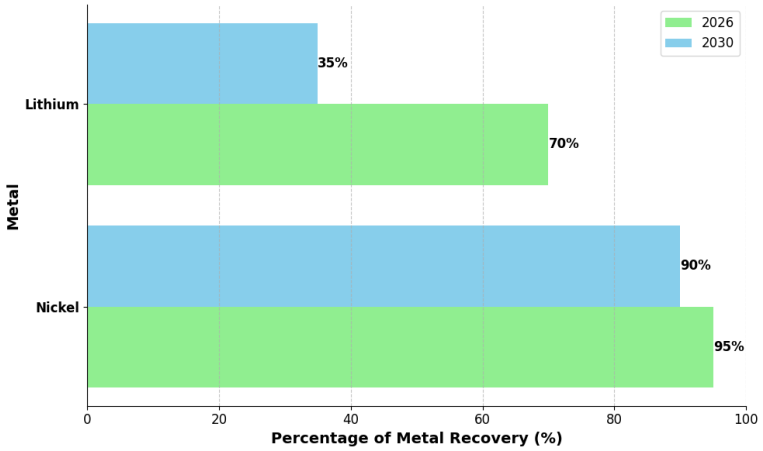

Figure 1.1: Metal recovery targets from spent LIBs for 2026 and 2030, as put forward by the European Commission.

Interestingly, figure 1.1 showcases that the recovery targets set for the lithium metal are lower than those for cobalt, implying that the recovery of some metals require more challenging recycling solutions. Furthermore, the targets displayed in figure 1.1 are augmented with goals set for the fraction of refurbished metal, that must in-future be present in newly produced LIBs. These state, that by 2035 hot of the press lithium-ion batteries should consist of 10 and 20 percent refurbished lithium and cobalt respectively [13].

Before the recycling goals can be achieved, however, a total of economic and technological obstacles should be overcome. As most of these obstacles stem from limitations imposed by present-day recycling technology a brief description hereof is required.

To begin with, the techniques currently being implemented at an industrial scale to recycle LIBs are diverse in nature. The exact selection and order of these techniques is unique for every company, just as the purity and type of material recovered is dependent on the path chosen. Therefore, to make a generic summary of the drawbacks of present-day recycling techniques would be inappropriate. Rather, a categorization of various methods should be completed and analyzed individually. In scientific literature, such a categorization is encountered in the form of one of the following three approaches: the pyrometallurgical, hydrometallurgical and direct recycling approach. An overview of how these approaches fit into the wider context of a lithium-ion battery's life cycle is portrayed in figure 1.2.
The pyrometallurgical approach is currently the most widespread approach to recycle LIBs. It utilizes thermal treatment of the battery material in order to decompose it into a metal alloy and slag [5]. Whilst the alloy, often rich in Cobalt, enables subsequent regeneration of the metal, the lithium-containing slag requires an extra hydrometallurgical procedure in order for the lithium to be recovered. Therefore,

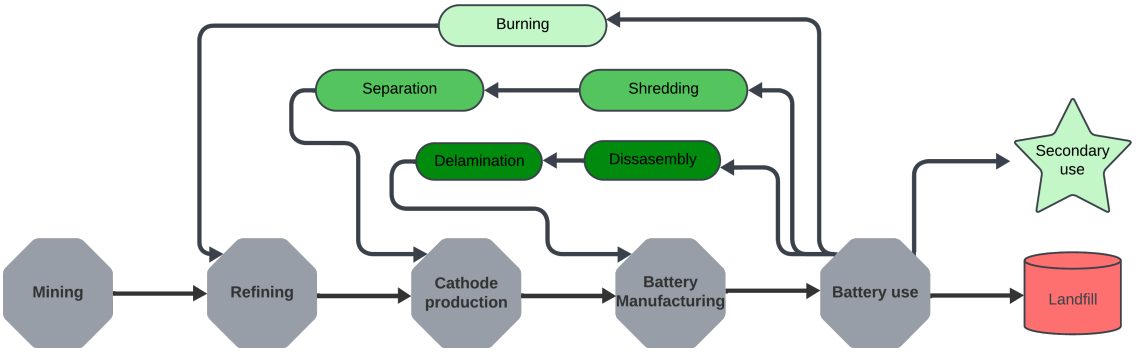

Figure 1.2: LIB production and recycling routes. The upper loop refers to the pyrometallurgical recycling technique. The middle loop, which includes the shredding and separation steps, refers to hydrometallurgical recycling. The lower loop, which includes the dissasembly and delamination steps, refers to the direct recycling approach.

implementation of the pyrometallurgical recycling route alone is unlikely to lead to the required recycling improvements.

The hydrometallurgical approach, used either in sequence with pyrometallurgy or implemented directly, involves the leaching of battery material in order to produce a mixture suitable for refinement through chemical methods. The issue with this approach is its dependence on expensive and polluting reactants, the circulatory of which are poor [14].

The last category for LIB recycling is the direct recycling approach. This approach involves manual disassembly of the LIBs and regeneration of valuable solid material through either solid-state or hydrothermal relithiation [15]. Whilst this technique is efficient in terms of energy consumption and allows for the largest variety of materials to be recovered, it is highly reliant on a significant amount of human labor. Without an immediate prospect on potential automation of this initial step, the scalability of direct recycling will remain to be an significant drawback.

In conclusion, no approach is currently capable of recycling battery material in an environmentally friendly, economically feasible and scalable manner. Even though some approaches have significant advantages over others, its larger implementation is inevitably disrupted by a limitation specific to that particular technique. Without an immediate breakthrough in one of the current recycling approaches, or the development of an entirely new recycling strategy, the high contrast between the recycling targets set by the European Commission and the disproportionately smaller present-day recycling capacity will remain to be a cause for concern.

1.3. Research strategy and questions

The research strategy utilized in the course of this research consists of three main parts. At first, a literature review is conducted into potential areas of improvement within the three main LIB recycling approaches. In doing so, special attention is given to the feasibility and prospects of emerging technologies at both industrial and laboratory scales. Eventually, the literature review identifies the excessive and non-circular consumption of acids within the hydrometallurgical recycling approach as the promising area for improvement and puts bipolar membrane electrodialysis (BPMED) forward as a viable respective solution. The investigation of how BPMED can be implemented effectively is hence regarded as the main focus for the remainder of this research.

The second part of this research focuses on the development and testing of an experimental setup for the BPMED. In the beginning phase of this step, different design considerations are examined and various protocols and procedures are established. In the middle stages of this part of the research miscellaneous issues associated with a flawed initial design are solved through various troubleshooting methods. Finally, in latter stages a central technological crux, inherent to the use of BPMED in the context of the hydrometallurgical recycling approach is identified. Specifically, this crux refers to the tendency of divalent metal ions to precipitate non-acidic media. To counter this crux, the study

proposed to use Donnan Dialysis as an effective method to control the acidity of the solutions within different electrodialytic compartments, which further narrows the focus of this research.

By the third and final part of this research, the experimental design is made free of any major issues and is primed for optimization. From this optimization, parameters required for further feasibility calculations are extracted, which in term are used to determine the extent to which BPMED can effectively be used to recycle LCO cathode material.

In summary, the overall objective of the research presented in this report is to improve upon the current state of LIB recycling technology. It does so by identifying potential areas of improvement in the existing recycling methods and investigates their respective solutions. Once BPMED is put forward as the most promising candidate for this aim, the goal of the research narrows to investigate the technological crux that would be responsible for the method's successful implementation. A formulation of which, is established in the following research question:

How to utilize bipolar membrane electrodialysis as a tool to recover lithium and cobalt from leached LCO cathode material?

Accompanying the main research question are the following explicitly formulated subquestions, constructed to guide the development of a targeted and structured response:

- *What are key challenges, associated with the utilization of BPMED for the recovery of lithium and cobalt from leached LCO cathode material?*
- *How can Donnan Dialysis be utilized in a BPMED setup in order to effectively vary the acidity of different electrodialytic compartments?*
- *What are key factors associated with recovery performance of BPMED in the context of lithium and cobalt recovery from leached LCO cathode material?*

2

Literature study

Having robust knowledge of the context in which the research presented in this report has been conducted is crucial for a proper understanding of the motivation behind various pivotal choices realized in subsequent stages of this study. Therefore, a literature review of the most important developments in the area of LIB recycling technology has been conducted and displayed in the present chapter. The review begins with a study of the structure of a LIB, its working principles and degradation mechanisms. Next, the review investigates the most promising state-of-the art recycling technology at both industrial and laboratory scales, whereby special focus is given to the advantages and drawbacks of each respective technique.

Once the excessive consumption of acid within the hydrometallurgical recycling route is identified as a potential area for improvement, the review shift its focus to a study of electrochemical methods, specific to the resolution of this issue. Thereafter, the review then proposes its own solution, one that indirectly encompasses a the use of a variety of previously identified methods. To be specific, the study notes that standalone use of Donnan Dialysis in order to create a closed-loop cycle for the acid consumed in hydrometallurgy is ineffective. When coupled with electrodialytic techniques, however, the downsides of the standalone technique should be reduced, leading to the proposition of the solution presented in the final stage of the literature review.

2.1. Lithium-ion cell

A conventional lithium-ion cell can be subdivided into three main components. As is displayed in figure 2.1. These components are a negative electrode (anode), positive electrode (cathode) and an organic liquid electrolyte. Through what is sometimes referred to as the ”rocking chair” mechanism Lithium-ions swing between the anode and cathode, just like a rocking chair swings from side to side [16]. In doing so, a chemical process called intercalation is utilized, in which Li-ions are inserted into the crystal structures of the host electrode materials.

Intercalation also gives rise to a number of electrode requirements. For instance, the anode should have minimal volume expansion and stress associated with it during charge/discharge. Likewise, cathode material should be able to react with lithium without changing host structure and contain a readily reducible/oxidizable molecule like a transition metal [16]. The combination with other basic requirements, such as good conductivity and stable operation under a wide temperature range adds to the complexity of cathode structures. An overview of the most common cathode structures are displayed in table 2.1.

As lithium-ions flow from the anode to the cathode, electrons are driven through an external circuit, generating an electric current. The half-cell reactions at the anode and an LCO cathode, as well as the overall cell reaction, are expressed by Equations 2.1b, 2.1a, and 2.1c, respectively.

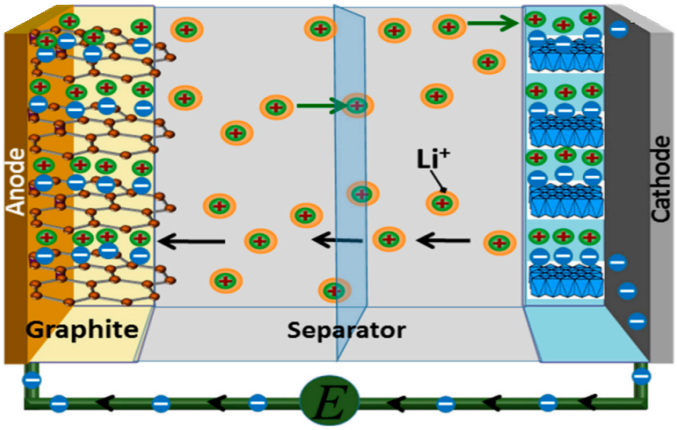

Figure 2.1: Simplified schematic of a lithium-ion battery cell, including the following main components: anode, cathode and separator. Lithium-ion flow and electron flow during discharge is represented by black arrows.

Table 2.1: Common cathode compositions for lithium-ion batteries, including a structural representation and summary of primary features.

Configuration	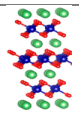			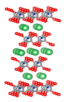	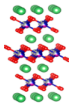
Structure	LCO	LFP	LMO	NCA	NCM
Composition	$LiCoO_2$	$LiFePO_4$	$LiMn_2O_4$	$LiAl_xCo_yNi_{1-x-y}O_2$	$LiCo_xMn_yNi_{1-x-y}O_2$
Primary features	Good structural stability and high capacity retention rate. Structure is often utilised in EVs	Best cycling stability, utilised in Tesla EVs.Poor performance in cold conditions.	Low capacity. Viable from an economic perspective	High capacity, high degradation rate	High capacity, high degradation rate

$$LiCoO_2 \rightleftharpoons Li_{1-x}CoO_2 + xLi^+ + xe^- \tag{2.1a}$$

$$xLi^+ + xe^- + 6C \rightleftharpoons Li_xC_6 \tag{2.1b}$$

Combining to get the overall cell reaction:

$$LiCoO_2 + 6C \rightleftharpoons Li_{1-x}CoO_2 + Li_xC_6 \tag{2.1c}$$

2.2. Degradation mechanisms

Degradation mechanisms in LIBs are a serious contributor to their poor circularity. The working lifespan of batteries in EVs, as a consequence of degradation mechanisms, are estimated to be around 10 to 15 years. At present, the main causes for LIB degradation are the occurrence of the following: ”parasitic reactions, cation mixing, active material dissolution and oxygen release” [17]. Furthermore, these causes for degradation are worsened by the presence of impurities [17]. Extensive research is being conducted into the mitigation of the parasitic reactions, such as the inclusion of additives into the electrolyte [18]. In addition, potential new anode and cathode structures are being investigated [19]. Nevertheless, the complex prerequisites of the electrodes and yet inevitable degradation of LIBs make the prospect of significant improvement in circularity through means other than recycling unlikely.

2.3. LIB recycling: publication trends

The methods aimed at recycling LIBs are diverse and unique for every company. The majority of recycling procedures, however, stem from similar working principles. Moreover, it is commonplace to find

overlapping steps within the different recycling routes. As a result, recycling techniques are typically classified into one of three main approaches: pyrometallurgical recovery, hydrometallurgical recovery and direct recycling. In a scarce amount of cases the categorisation expanded with the mechanochemical approach [20].

Furthermore, it is important to stress that some particular metals aren't recovered through one approach only. Rather, a combination of approaches is required, as shown by figure 2.2. In particular, the figure displays the number of publications made between 2010 and 2020, showcasing potential for the implementation of a combination of approaches, as apposed to their singular use [21].

Figure 2.2: Number of publications associated for LIB recovery made between 2010 and 2020, categorised by metal. Hydrometallurgical recovery is shown in blue, pyrometallurgical in yellow and the combination of the two in purple.

It should, however, be noted that figure 2.2 fails to take into account publications associated with the direct recycling approach, which has also been integrated with the approached shown in other research.

2.4. The pyrometallurgical recycling approach

At present, pyrometallurgical recycling is the dominant approach for LIB recycling [22]. It has proven to be successful in recovering a number of metals, including Cobalt. Furthermore, off-gas treatment improvements, like those for hydrogen fluoride, have strongly decreased the environmental impact [5] of the approach.

In basic terms, metal recovery in pyrometallurgy is achieved through the implementation of a thermal treatment [23]. Whilst a number of different pyrometallurgical routes exist, its products primarily consist of a metal alloy and slag. The alloy contains a majority of the transition metals originally present in the cathode structure, whilst lithium oxide is contained within the slag. For a number of metals, including lithium, additional hydrometallurgical recovery is required in order to achieve recovery.

Furthermore, mechanical or thermal pretreatments of LIBs are often implemented in order to increase recycling efficiency and decrease environmental impact [2]. In a thermal pretreatment, organic binder material and carbon is effectively removed, which would have otherwise absorbed valuable Lithium and decreased the recovered lithium fraction in subsequent steps. Furthermore, thermal pretreatment offers "a controlled deactivation and safe decomposition of the combustible organic component of the LIB" [5, 24]. Finally, thermal pretreatment can ensure safe battery discharge, which decreases the possibility of adverse chemical reactions and spontaneous combustion due to an accidental short-circuit [5, 25–27].

The main thermal pretreatments are incineration and pyrolysis. Whilst both approaches serve a similar purpose, there is a significant distinction between the two. In the case of incineration, oxygen or air has to be present throughout the burning procedure [27]. Meanwhile, the opposite condition is required for pyrolysis [28, 29].

The main step in the pyrometallurgical approach is often referred to in literature as extractive pyrometallurgy. It most commonly encompasses the utilisation of one of the following techniques: calcination or roasting, followed by smelting. In practice, these techniques can be implemented within the same furnace, divided into different levels. A summary of the working principles of these techniques is provided next.

Calcination
A review on calcination has previously been conducted by Yin and Xing. Yin defines calcination as "the thermal treatment process for solid materials that involve thermal decomposition, phase transition, or removal of volatile substance in the absence or limited supply of air or oxygen" [23]. The calcination path tends to pursue the following reaction route:

$$\text{Solid A} \rightleftharpoons \text{Solid B} + \text{Gas} \tag{2.2}$$

In reaction 2.2 solid A refers to the cathode structure, solid B to the desired metal oxide product. The gas in figure 2.2 is dependent on the cathode structure used. For LCO cathode material the CO_2 gas is produced, whilst for the case of LFP more toxic PF_5 is generated [23].

Roasting
Similar to the incineration process, conventional roasting involves the heating of battery material in the presence of oxygen or air [23]. In many industrial cases, however, a variation of this technique is implemented called reduction roasting. This technique involves the addition of a reducing agent to the overall process, such as coal or carbon, in order to reduce cathode material to a lower valence state, which eases subsequent separation [5, 30].

Smelting
After metal oxides have been produced in the roasting or calcination step, their subsequent conversion is commonly achieved through smelting. Whilst there are a number of variations of this technique, such as flash smelting, a typical pyrometallurgical process involves reduction smelting. This type of smelting involves a reducing agent, such as natural gas, carbon or carbon monoxide, and a flux. The overall process is represented in equation 2.3 [23].

$$\text{Oxides + reducing agent} \rightleftharpoons \text{alloy + slag + gas} \tag{2.3}$$

Pyrometallurgy: A discussion
The goal of this section is to utilize the knowledge acquired in preceding parts of this chapter in order to progress on the main objective of this report. Which in part is, to identify potential areas of improvement in the existing recycling methods and investigate their respective solutions. These areas will be identified through considerations of both economic and environmental arguments.

To begin with, the economic viability of the pyrometallurgical approach is strongly dependent on the type of cathode structures that are being recovered, as concluded by Reinhart et al. [31]. This conclusion is in line with the previously mentioned theory, which states that some desired metals in the pyrometallurgical approach, such as cobalt and nickel, are yielded in the metal alloy; whilst other materials contained within the slag require further separation procedures. Unsurprisingly therefore, only cobalt and nickel rich cathode structures are suitable for pyrometallurgical recovery from an economic perspective.

For the development of the environmental argument, it is useful to establish that pyrometallurgy by itself is an energy intensive process, as the majority of its steps require operation at high temperatures. However, it should also be noted that the energy requirement for the recovery of cathode material through

this approach is nevertheless significantly less than that of the production of virgin cathode material [32, 33]. Meaning, that at least in terms of energy consumption of the physical process, pyrometallurgy has the potential for a net positive environmental impact.
The environmental impact expressed in terms of carbon footprint is nonetheless negative.This stems from the fact that various gases produced throughout the process, when converted to their CO_2 equivalent, contribute to a total carbon footprint of around 10 kg of CO_2 equivalent per kg of battery material [34]. A value similar to that of cathode production from primary resources.

On a new note, pyrometallurgy lowers water depletion and freshwater contamination. It also avoids political issues associated with Cobalt mining, as mentioned in the introduction.

Overall, the scalability and economic viability of pyrometallurgy for a number of metals make its continued utilisation in the context of LIB recycling in the future likely. However, the approach has some major drawbacks. Firstly, the carbon footprint of the approach doesn't beat that of virgin cathode production. Secondly, pyrometallurgy is unable to recover lithium. Therefore, it is safe to conclude that pyrometallurgy may play a role in the future or LIB recycling, but only to a limited extent in the former steps of the process.

2.5. The Hydrometallurgical recycling approach

As briefly mentioned in the introduction, the hydrometallurgical approach may be used in sequence with extractive pyrometallurgy or be implemented as a stand alone method. In this section a brief summary of the over process is given, followed by an overview of recent advances within the various hydrometallurgical process steps.

A hydrometallurgical recycling route involves the dissolving of metal, mainly cathode material, by an acidic or basic medium, "which provides an aqueous form of raw material for subsequent separation and purification" [20]. Most commonly these steps involve "sedimentation, precipitation or solvent extraction" [14]. On a laboratory scale a number of electrochemical methods, such as electrochemical deposition and Donnan dialysis have also proven to be successful in recovering metallic compounds, as will be discussed in chapter 2.7.

Leaching
The leaching of the cathode material may be achieved through the utilisation of both organic acids and inorganic acids, as well as ammonia-based compounds [20]. In addition, the leaching step can be divided into two categories: non-selective and selective recovery [35]. The distinction arises from the fact that non-selective recovery targets all of the cathode, whilst selective recovery dissolves one metal into the solution only, most commonly Lithium. An example of a selective leaching reaction is given by equation 2.4, in which LFP cathode material is leached with sulphuric acid. Note that in this reaction hydrogen peroxide is added as an oxidising agent in order to increase the selectivity towards lithium recovery [35].

$$4\mathrm{LiCoO_2(s)} + 12\mathrm{HNO_3(aq)} \rightarrow 4\mathrm{LiNO_3(aq)} + 4\mathrm{Co(NO_3)_2(aq)} + 6\mathrm{H_2O(l)} + \mathrm{O_2(g)} \tag{2.4}$$

The leaching step is financially demanding, primarily due to the significant amounts of acid required [12]. Furthermore, the step has a negative environmental impact due to the unavoidable disposal of high volumes of acidic leachant. In order to decrease the ecological impact of the process various studies have been conducted into the utilization of organic acids, which strongly reduce pollution through biodegradability. Examples of such acids are: citric acid, malic and acetic acid. However, these acids have worse chelating ability compared to inorganic acids and are more expensive.

Recovery
In a typical hydrometallurgical process the metals are subsequently separated from its leached solution through chemical precipitation, solvent extraction or a combination of both.

In chemical precipitation, which is the more dominant technique, calculated alterations in parameters such as pH and/or temperature, change the solubility of the metal salt in the leached solution. Commonly, however, the technique does require further addition of anions in order for the precipitation to take place [20].

The solvent extraction technique utilises a special liquid extractant, in which the solubility of the metals differ from the ones in their original solution. Whilst this technique omits additional use of acid, it suffers from similar drawbacks. Namely, the extractants are costly and disposal regulations must be complied with in order to avoid environmental pollution.

Hydrometallurgy: a discussion
Having provided the reader with an overview of the overall concept of hydrometallurgical LIB recycling, a critical review of the effectiveness of the process may be introduced.

Starting with the financial discussion, the economic feasibility of the hydrometallurgical approach is strongly dependent on a total of the following costs: inorganic/organic acids, reactants in the pretreatment and recovery steps, and the primary metals themselves. A few studies have confirmed the economic feasibility of the typical hydrometallurgical approach, though often omitted labour and overhead costs. For instance, Thompson et al. established that the hydrometallurgical route involving: shredding of battery material, separation of the crushed material, leaching and recovery; may lead to a 20 % higher profit margin when compared to virgin cathode production [12]. The implications of this claim are significant, as few other studies have confirmed that higher recovery rates, associated with shredding, outweigh the added expenses of the increased number of separation steps.

Moving onto the environmental discussion, hydrometallurgical recovery seems to solve many issues associated with the previously discussed pyrometallurgical alternative. For starters, hydrometallurgy enables the recovery of all metals contained within the cathode structure, including lithium. Secondly, the right pretreatment of battery material can decrease the production of toxic gases in the leaching step, aiding a decrease in carbon footprint of the recycled material. In fact, for certain cathode structures, such as NMC, the decrease can yield values around 10-20 % lower compared to pyrometallurgical recovery. The third and perhaps most important environmental benefit of this approach, is the enabling of lithium production with substantially lower water usage. In the context of primary lithium extraction from brines, water usage is a major topic for discussion.

Having mentioned the advantages of this approach, potential areas of improvement may be identified. At present, the hydrometallurgical approach has a number drawbacks, most of which stem from the non-reuse of reagents in pretreatment, leaching and recovery steps. Examples of these instances are leaching acids, such as hydrochloric or nitric acids, and solvent extractants, such as N-methyl-2-pyrrolidone (NMP). Not only are these reagents hazardous and require proper disposal, they have a major impact on overall profitability. In fact, the leaching and recovery reagents alone may amount to as much as 50 % of the total recycling cost, depending on the exact hydrometallurgical route chosen [12]. Looking at this critically, one may conclude that the development of an alternative solution to these steps would contribute to major economic and environmental benefits.

One improvement to the leaching step has already briefly been introduced in this chapter under the header ”Leaching”, which notes that environmentally unfriendly acids may be substituted by biodegradable, organic acids. Whilst this would strongly improve hydrometallurgy from an environmental point of view, the economic feasibility of this substitution demands further investigation. Nevertheless, it is noted that leaching and recovery steps within the hydrometallurgical approach remain to be potential areas for improvement and more alternative solutions will be presented in later sections of this report.

2.6. The direct recycling approach

Another number of recycling techniques fall into the category of direct recycling. Noteworthy, the variety of these techniques is quite broad, which makes the outlining of a typical direct recycling case challenging. Moreover, in a number of scientific articles proposed direct recycling steps overlap with

steps in pyro- and hydrometallurgical routes. These instances are especially prevalent in the beginning phases of LIB recycling. Contrary to the hydrometallurgical approach, direct recycling omits chemical transformations of the cathode structures, other than the ones present in the final regeneration step. Instead, the method encompasses the separation of cathode (and anode) material through mechanical separation techniques and thus enables direct reuse of materials in remanufactured LIBs [36].

Nevertheless, scientific literature commonly subdivides the direct recycling approach into three distinct steps. A simplified version of this process is portrayed in figure 2.3.

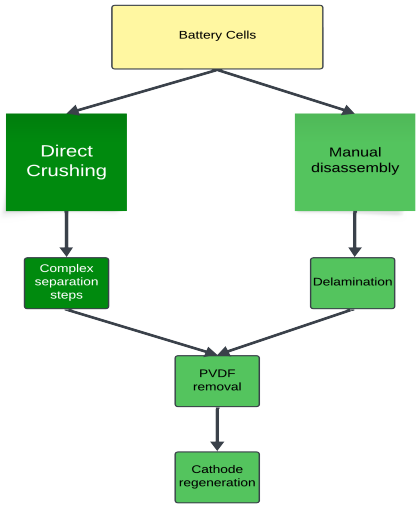

Figure 2.3: Schematic for the recovery of spent LIBs using a typical direct recycling approach.

At first, the cathode material is harvested through manual disassembly and delamination. Alternatively a combination of direct crushing with a variety of mechanical separation techniques are imposed. Examples of such techniques are pneumatic separation, eddy current separation, floatation, etc. Whilst direct crushing is considered to be a feasible step for large scale operation, the composition of crushed material after crushing is often complex and contains a large number of impurities [37]. This leads to complex subsequent separation and higher overall costs. Furthermore, in the processes gases containing electrolyte solvents and carbon dioxide are released, and thus require gas collection or treatment [15].

The binders and carbon are removed from the mixture. At present, thermal treatment is regarded as only feasible option for the removal of PVDF [38]. Although other techniques, such as the utilisation of molten salt and other solvent extractants, are under investigation.
Lastly, in a typical direct recycling approach the extracted cathode material is regenerated through either solid-state or hydrothermal relithiation. In solid-state relithiation spent LCO CAMs are calcinated directly with lithium carbonate, lithium nitrate or lithium hydroxide. Hydrothermal relithiation on the other hand, uses ”lithium hydroxide solution as a resource, and it is commonly followed by an annealing process” [15].

Direct Recycling: A Discussion
From an environmental standpoint, the direct recycling approach is the most effective approach to date. It uses neither the polluting roasting and calcination steps of the pyrometallurgical approach, nor the leaching step within the hydrometallurgical one. Furthermore, through direct recycling high recovery rates can be achieved of almost all battery elements, not just those contained within the cathode structures.

Nonetheless, it remains to be seen whether direct recycling will become the dominant approach in the future of LIB recovery. The reason for this is twofold. For starters, the potential financial gain

from higher recovery rates needs to outweigh the increased disassembly costs associated with this approach. Improvements of this outcome would likely stem from advancements in scalability through robotic automation, the prospect of which strongly depends on the standardisation of a lithium-ion battery. Next, the probability of such a standardisation is strongly reliant on government organs to enforce the required legislation.

In conclusion, whilst the direct recycling approach has the potential to become the most viable recycling option for LIB recycling in the future from both environmental and financial viewpoints, its immediate large-scale deployment seems improbable. Ergo, in the remainder of this report emphasis is laid onto finding other alternatives to the previously identified technological crux. Namely, the leaching and recovery steps within the hydrometallurgical method.

2.7. Electrochemical methods for LIB recycling

The previous chapter has layed emphasis on the drawbacks associated with the hydrometallurgical leaching and recovery steps. Thereafter, potential solutions to these issues have been explicitly proposed through the use of a direct recycling approach. Whilst this approach successfully omits the use of expensive and environmentally harmful leachant, it suffers greatly from scalability issues. Hence effort into other alternative solutions to the conventional hydrometallurgical recycling route is required. This chapter explores the techniques aimed at improving the leaching and recovery steps directly through the utilization of electrochemical technology.

Electrochemical methods for primary sources

To begin with, it is worth mentioning that electrochemical methods have applications in metal extraction from primary sources as well as secondary ones. Motivation for investigation into electrochemical applications in the context of primary sources is twofold. Firstly, the process could generate ideas that would translate to uses in the area of LIB recycling. Secondly, as mentioned in previous chapters, the effectiveness of recycling technology is strongly dependent on the economics of mining battery material from primary sources. If electrochemical methods manage to significantly improve the economic feasibility of the mining process, assumptions about the financial targets associated with LIB recycling need to be reevaluated.

Electrochemical methods for secondary sources

A significant amount of literature has been published on the utilization of electrochemical techniques aimed at improving the leaching and recovery steps in standard hydrometallurgical recycling. With this, a substantial amount of publications claim to have developed closed loop systems that completely bypasses the generation of acidic waste.

Electrodeposition

Cerillo-Gonzales et al. proposed precipitation electrodialysis as shown in figure 2.4 to recover Li and Co. The process utilizes a Neosepta CMX-fg standard grade cation exchange membrane. In the process black mass is directly leached in the vessel, pumped through the stack where Li and Co is deposited onto the cathode, and recycled back into the container [19].

However, the process way only able to extract 33 % of Cobalt and 62 % of Lithium, which isn't in line with the targets set by the European Comission as discussed in section 1.2. Furthermore, the process is slow, amounting to a total of 3 days. Finally, the process is a batch process, whereby the deposited materials require removal from the cathode. Therefore this research concludes that electrodeposition is unsuitable for large-scale operation.

Slurry Electrolysis

Li et. al. have developed a recovery method for lithium and manganese from scrap $LiMn_2O_4$ by means of slurry electrolysis. This method, as shown in figure 2.5, combines leaching, solution purification, electrowinning and electrodeposition into a single step [39].

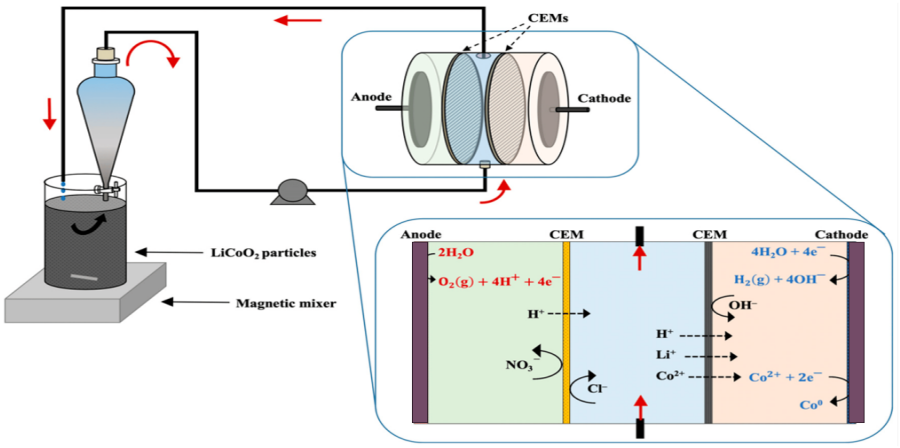

Figure 2.4: Schematic for the electrodeposition process as proposed by Cerillo-Gonzales et al. Leaching of the $LICoO_2$ occurs in the vessel, after which the mixture is pumped through the cell.

LMO cathode material is suspended into an electrolyte solution mixed with H_2SO_4 and $MnSO_4$. After the application of an electric current Li+ and Mn2+ ions are transported through the filter cloth to the opposite electrode, where Mn is deposited as MnO_2 and the lithium ions remain in solution. Subsequently, the MnO_2 is filtered out and the Li+ through evaporation after addition of Na_2CO_3.

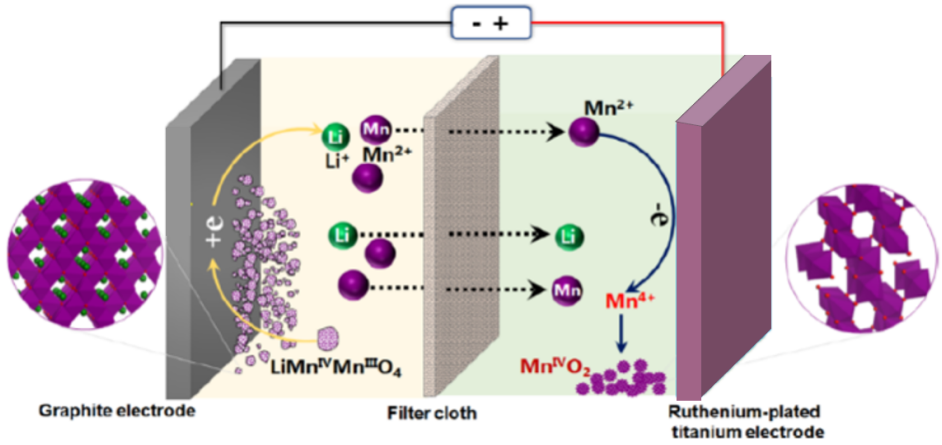

Figure 2.5: Slurry electrolysis diagram, as proposed by Li et al. Leaching of the LMO cathode materials occurs at the cathode, before it is transported through the filter cloth and deposited at the anode as Mn^4O_2, whilst the lithium remains in solution.

Whilst the Li et. al. correctly suggests that the process is ”economically feasibly, environmentally friendly and has great potential for the recovery of other scrap cathode metals”, it scalability potential remains to be investigated.

Donnan (diffusion) Dialysis

Sonoc et. al. have developed a method to recycle Lithium and Cobalt from spent lihtium ion batteries using Donnan dialysis [40]. Donnan dialysis relies on an chemical potential gradient as the driving force to separate ions from a solution, with a possible, often low, electric potential acting in the opposing direction. In the proposed approach a leachate containing Co, Ni, Mn and Li salts are pumped through a series cation exchange membrane containing cells, each utilizing Donnan dialysis to achieve separation.

Whilst the approach effectively simulates high recovery efficiencies for different transition metals (above

90 %), the approach suffers from a number of serious issues. Firstly, the approach is slow. The Donnan Dialysis recycling route, as proposed by the study, requires a minimum of 2 days before it achieves the desired separation. The second issue isn't mentioned directly in the published study, but, to the best of our knowledge, must be inherent to the design. The issue is that, within the proposed recycling route, a monovalent cation exchange membrane must be utilized in order to separate lithium ions out of the leached solution into a product compartment. In doing so, proton diffusion from the feed to product compartment is inevitable, making efficient acid recovery practically impossible [41].

Electrodialysis coupled with chelating agents

A number of studies, such as the ones conducted by Iizuka et al. and Chan et al., have attempted to use electrodialysis in order to separate monovalent and divalent ions, often found in different LIB cathode structures, from each other [42][43]. The working principle behind these studies is displayed in the form of a sketch in figure 2.6.

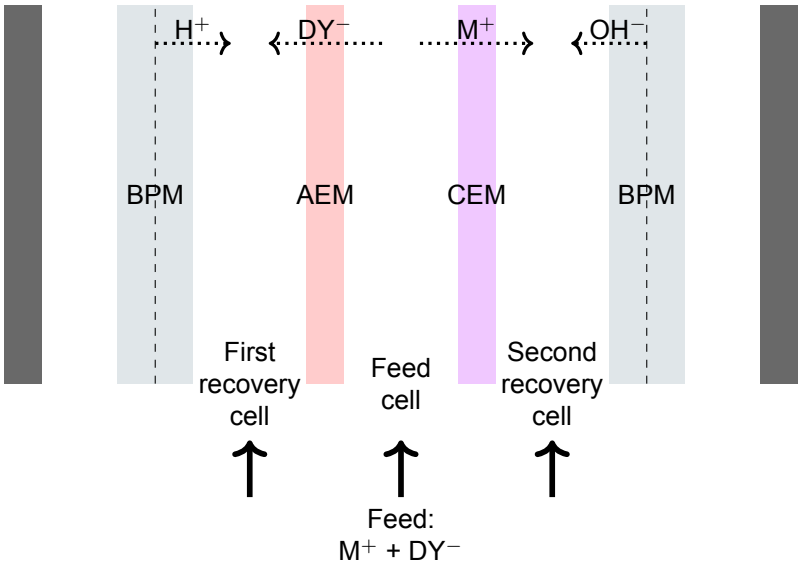

Figure 2.6: Separation of cobalt and lithium with by means of electrodialysis, coupled with the use of chelating agents. The cathode is displayed by the gray vertical bar on the right side of the figure, whilst the anode is represented by the same shape on the left. Monovalent ions are displayed as the symbol M, divalent ions as D and the chelating agent as Y.

In figure 2.6, monovalent cations, such as lithium, are represented by the symbol "M^+". Meanwhile, divalent cations, such as cobalt or nickel, are represented by the symbol "D" and the chelating agents are represented with the symbol "Y". Next, the figure displayed how the monovalent metal ions and the chelated divalent ions are fed into an electrodialytic setup, where the two are subsequently separated into their respective recovery compartments.

Both works have achieved high recovery efficiencies for the different metals, as well as successful recovery of different chelating agents. Nevertheless, the studies suffer from a similar and substantial drawback. Namely, that the the chelating ratio of divalent to monovalent ions is strongly influenced by the pH of their respective solution. For instance, according to IIzuka et al., the pH of a solution containing both cobalt and lithium should remain above 4 in order for cobalt to be chelated and the lithium to retain its monovalent form. This issue suggests, that the pH of the leached feed solution should be increased before it is supplied to the electrodialytic setup, harming the prospect of efficient acid recovery.

Secondly, the solubility of chelated compounds is also strongly dependent on the pH. Chan et al. has reported to use sulfuric acid in order to bring the pH of the chelated cobalt compound below 0.5, in order to precipitate the compound as an inteermidiate product. In the context of hydrometallurgical recycling, this pH is higher than the pH required to achieve efficient leaching efficiencies, as proven by Lee and

Rhee. To be precise, their work showed that the leaching efficiency of LCO cathode material at a pH of 0.5 is about 40 % for both lithium and cobalt, a value that is almost doubled when acid with a pH value of 0 are used instead [44].

Electrochemical methods: A discussion
The section provided an overview of recent developments in the utilization of electrochemical methods in the context of battery recycling. The main motivation for these developments was to solve the environmental and economic issues associated with the use of leaching agents required for the otherwise promising hydrometallurgical approach. Furthermore, electrochemical methods have historically shown to have good scalability, suggesting that it's integration with other pyro- and hydrometallurgical steps could potentially outperform direct recycling solutions, discussed previously in section 2.6. These, in turn, have also successfully omitted the leaching step, but are in need of special pre-treatment, the scalability of which is limited by challenges in automation.

The electrochemical methods discussed in this section have, for the most part, been able to achieve good metal recovery efficiencies. Moreover, Li et al. and Sonoc et al. have succeeded in the recovery of leaching agent, thereby effectively solving the issues associated with its excessive utilization within the standard hydrometallurgical approach. Nonetheless, no method has yet been able to have a total of: good recovery efficiency, good scalability and efficient leaching agent usage. Meaning, more research has to be conducted into alternative solutions to the crucial leaching step.

3

Proposed solution

By building on previously identified electrochemical methods in chapter 2 and carefully examining their respective advantages and drawbacks, this chapter proposes the use Bipolar Membrane Electrodialysis (BPMED) in combination with Donnan Dialysis as a means to improve upon the classical hydrometallurgical recycling route. To a small extent, the solution presented in this chapter is an incorporation of the work conducted by Sonoc et. al., which investigates the potential use of Donnan dialysis in the context of LIB recycling, into the works of Makuza et. al. and Chan et al., which put forward different variants of electrodialytic setups in successful attempts to separate chelated metal ions from their respective acidic solutions.

Having said that, the review notes that the works by Makuza et. al., Ilzuka et al. and Chan et. al., on their own, fail to provide a closed-loop pathway for the leaching acid. However, when combined into a separate system, have the potential to be effective. As discuss is in section **??**, the main technological obstacle that the work of Makuza et al. and Ilzuka et al. have proven to be limited by, is the tendency of the chelating agents to precipitate in strongly acidic environments. Furthermore, these studies have shown that chelating agents are likely to attach to monovalent ions instead of the divalent ions in acidic environments. Implying, that before leached cathode material can be fed into one of the electrodialytic setups, the acidity of its respective solution must be increased. Essentially, this makes effective recovery of leaching acid impossible. Finally, the review notes that the Donnan Dialysis method, proposed by Sonoc et al., is constrained by the unavoidable diffusion of protons from the leached feed cell into the respective lithium recovery cell, causing the the same issue.

A sketch of the proposed solution is displayed in figure 3.1. It consists of four distinct flow channels, separated by different ion exchange membranes. Specifically: two bipolar exchange membranes, one anion exchange membrane and one cation exchange membrane. The center flow channel contains the feed solution, produced in advance through standard hydrometallurgical recycling techniques. In this research, the feed has been prepared through the leaching of pure LCO cathode material with 1 M nitric acid and 1.7 %vol hydrogen peroxide solution, as has been advised by in the study of Lee and Rhee [44]. Once the feed is supplied into the electrodialytic setup, an electric potential is applied. This forces cations, such as the hydrogen, lithium and cobalt to diffuse through the CEM into the metal product compartment, where they are subsequently are recombined with a hydroxide ion provided by the BPM. Simultaneously, the NO_3 anions are forced from the feed compartment into the acid recovery compartment, where they recombine the hydrogen ion produced by the BPM.

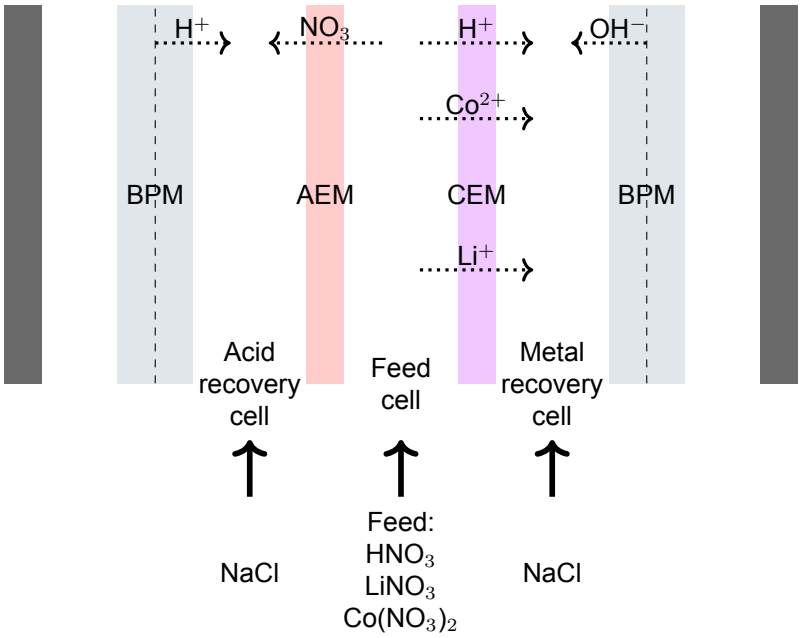

Figure 3.1: Sketch of the proposed solution. The cathode is displayed as a gray vertical bar on the right side of the figure, the anode is represented by the same shape on the left. Monovalent ions are displayed as the symbol M, divalent ions as the symbol D and the chelating agent as the symbol Y.

Moving on, the two flow channels on either side of the feed compartment contain a 0.5 M sodium chloride solution, whilst the electrode rinse compartment contains a 0.25 M sodium sulphate solution. The salt presence is required for the conduction of current, as well as the facilitation of Donnan Dialysis between the feed and metal recovery compartment, as is explained schematically in figure 3.2.

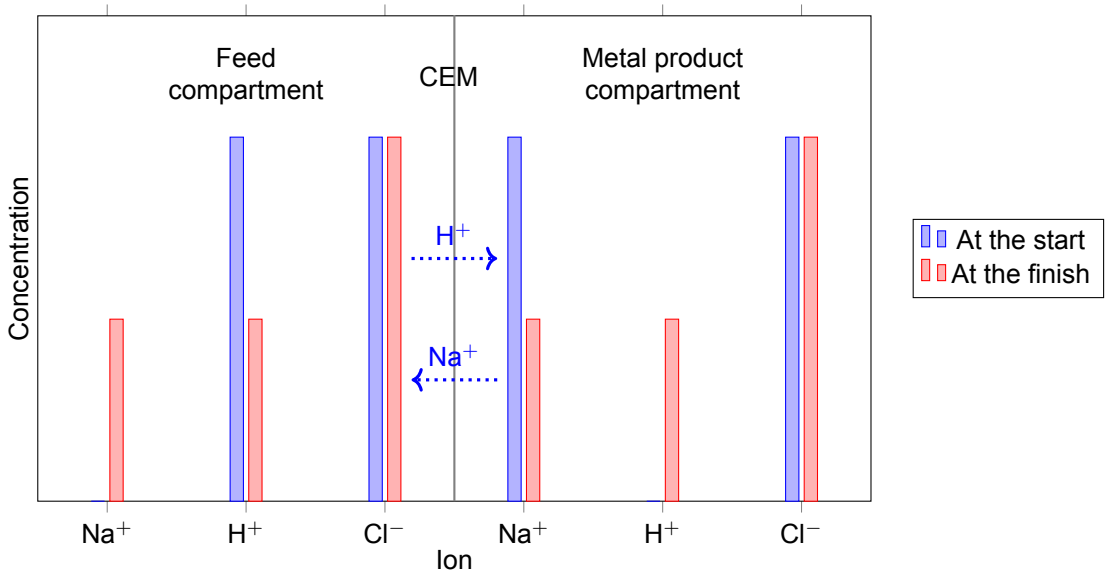

Figure 3.2: Visualization of Donnan dialysis effects through the CEM. The figure shows a section of the BPMED setup, displayed in figure 3.1. In the showcased process, Na^+ ions from the metal product compartment are interchanged with the H^+ ions from the feed compartment, effectively increasing the pH of its respective solution.

In figure 3.2, hydrogen ions diffuse from the feed compartment into the metal product compartment, decreasing the pH within the metal product compartment. Parallel to this, sodium ions diffuse from the

metal product compartment into the feed compartment, effectively conserving electroneutrality.

Apart from the pH adjustments, which result as a consequence of the Donnan Dialysis displayed in figure 3.2, other combinations of ion migration may occur, resulting in different pH changes. Four of these combinations are displayed explicitly in figure 3.3. Firstly, the figure shows how the pH in the acid recovery compartment may decrease due to simultaneous migration of both the NO_3 anion through the AEM, as well as leakage of $H+$ ions. What is most important in figure 3.3, is the diffusion mechanism shown within the top right circle. As OH^- ions get produced by the BPM during operation, these combine with H^+ ions, that diffuse through the CEM from the feed. As this happens, the pH within the metal product compartment stays constant. This poses an important optimization challenge, associated with the proposed solution. The Donnan Dialysis through the CEM, shown in the lower circle on figure 3.3 and in more detail in figure 3.2, should to some extent outweigh the diffusion of the H^+ and OH^- ions, displayed of the top right of figure 3.3. In an ideal scenario, the combination of these processes would lead to a pH within the metal product compartment of around 0.2. A condition, which allows for good cobalt salt dissolution.

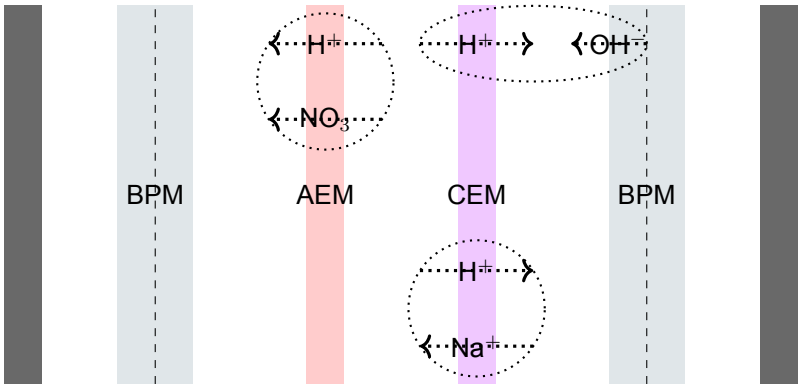

Figure 3.3: Visualization of the possible proton migration within the BPMED setup, sketched in figure 3.1. The dotted circles represent how the proton migration between compartments are counteracted by other charged ions in order to reserve electroneutrality. The ion migration in the top right ellipse showcases the effects of electro-osmosis. The bottom circle shows the effects of Donnan dialysis, mentioned in figure 3.2

3.1. Alternative solution

The electrodialytic methods, proposed by Ilzuka et al. and Makuza et al. seemed to omit the potential precipitation of metal material in their designs. Whilst the authors haven't stated the reason for this explicitly, it is reasonable to assume that the authors were caustious of a number of issues, associated with the precipitation.

Firstly, the precipitation could get stuck within the stack. If a particular entrance or exit is blocked, pressure can build up in the system, posing an immidiate danger. Secondly, without filtration or another separation method, small solid particles can irreversibly damage any pumps utilized during the experiment. Finally, to allow for the metal salts to precipitate, the flow compartments, stack inputs and outputs would have to be made bigger, decreasing the Faradaic effiency of the system due to increased ohmic losses. All in all, this review notes that the construction of an electrodialytic system, which allows for metal precipitation, is possible and deserves further investigation. However, for the purposes of this research, the focus is shifted completely to the solution proposed earlier in this chapter.

3.2. Design strategy

Complex technology can be developed through the use of different design strategies. A popular method is the so called ”scrum” method, whereby the complex design is subdivided into smaller parts. Subsequently, these smaller parts are tested individually, before integrated together into the larger complete system.

Alternatively, the complex system could be build directly, without the preliminary testing of individual components. Instead, this method relies heavily on troubleshooting solution of issues encountered in the final build.

Whilst the former method may, at first glance, seems like the safer and perhaps more promising option, the research conducted in this report follows the latter strategy. The reason behind this choice, is the fact that the proposed solution relies heavily on complex interaction between all of its subdivided parts. Apart from a verification of the healthy condition of the components, the scrum method would not act as a proper stepping stone to the final functioning of the setup.

Therefore, in the course of this research the BPMED system is build to completion early in the design process. Subsequently, initial design flaws are eliminated through rigorous troubleshooting methods, before a further optimization of the setup is performed.

4

Experimental design

4.1. Setup configuration and material selection

In this chapter the final equipment specifications are displayed, as well as an in-depth explanation as to how the various equipment choices have been realized. The goal of this chapter is to not only aid the reader in reproducing the research conducted in this report, but also to provide information on the utilized materials, their sizing and potential limitations.

Stack requirements:

- The stack has to be able to support a total of four inflow and four outflow channels.
- The dimensions of the stack should allow for easy installation within a fume hood.
- The stack should be easily repairable and allow for quick disassembly.
- Stack gaskets should be made from either EPDM or Viton rubber in order to comply with necessary resistivity to acidic and basic media.
- Flow chambers, screw connections, valves etc. should be resistant to highly acidic and basic media. Use of PVDF, PP or similar plastics are encouraged.
- The cell design should allow for a reasonable scalability analysis.

Electrode requirements

- Electrodes should allow for good conductivity and a uniform distribution of current density.
- Be highly resistant to acidic and corrosive media in case of unforeseen membrane leakages.
- Discourage electrodeposition of metal ions.
- Use of Platinum coated Titanium electrodes is encourages.

Ion exchange membrane requirements:

- All membranes should maintain operation capacity at a high pH stability range.
- Cation exchange membranes should enable transport of both mono and divalent. cations.
- Possible resistivity against small amounts of hydrogen peroxide is encouraged

Final design

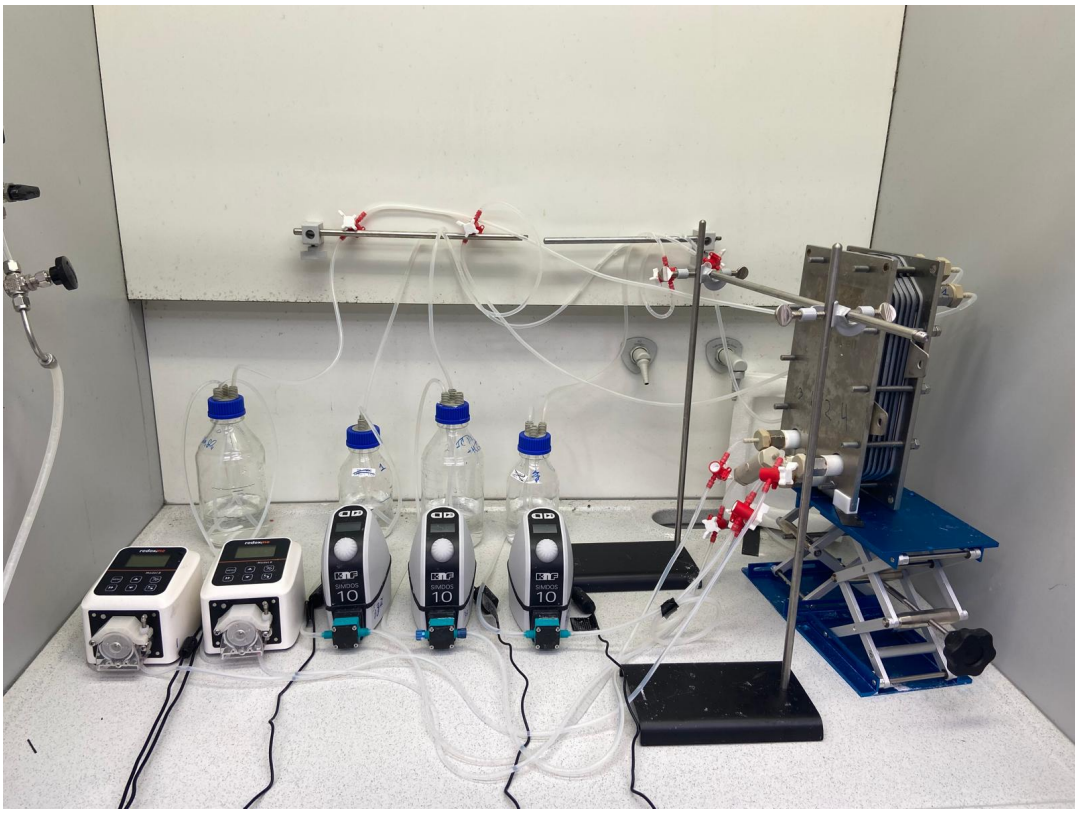

Figure 4.1: Final setup: the stack is located on the right, with it's flow inputs on the bottom and output flows on top; the input flows are connected to the pumps on the middle left of the figure. In turn, these pumps are connected to the four compartment beakers, located behind the pumps.

4.2. Potential hazard identification and safety protocol

In this section potential hazards during various phases of the experiments are identified. Also, the section provides an overview of the various safety protocols put in place to remove or minimize these dangers.

For starters, liquids utilized throughout the experiments are highly corrosive in nature. Whilst not posing an immediate danger if contained within the leak-tight experimental setup, precautions to avoid potential accidents should still be taken. In particular, the entire setup, including the stack and the pumps should be placed inside of a fume hood. This way unforeseen leaks (or even sprays) of harmful substances, caused by faulty tubing, broken pump connectors, or unforeseen pressure build ups within the stack cannot harm the individual conducing the experiment.

Having said that, it should be stated explicitly that thorughout the course of this research, there have been a number of occasions, whereby the connections between the tubes and the pumps, as well as the connections between the tubes and the cell were detached due to accidental build-ups within the cell. In some instances this happened when a tube accidentally folded somewhere in the system and thus prevented liquid from exiting the system. Shortly thereafter, the tubes would detach, leaking a notable volume of liquid.

The next considerable safety hazard arrizes from the fine nature of the solid cobalt salt precipitate. The inhaling of which, should be strictly avoided at all times, or done so through the use of an appropriate chemical mask.

In the context of this research, solid cobalt particles only pose a safety hazard during the repairing process of the cell. During this time precipitate isn't contained within a liquid and can therefore be inhaled.

Moving on, a number of gasses are produced throughout normal operation of the cell. Without any unforeseen side reactions at the electrodes, hydrogen production should occur at the cathode, whilst oxygen is produced at the anode. The combination of these gasses, just as their individual production, is highly flammable and appropriate ventilation measures should be taken.

Finally, it is important to discuss safety precautions surrounding the potentiostat. Whilst it is perhaps unwise to test this first hand, the potentiostat during operation isn't of lethal danger under normal (dry) circumstances. Looking at the numbers, the potentiostat is able to supply a maximum of 30 V. For an adult male, who's bodily electrical resistance amounts to an estimate of 10 kOhms, the potentiostat can supply a maximum of 3 mA, which would most likely cause a light shock. Nevertheless, the handling of the electrodes should be done with care and the voltage supply cables should be kept away from liquid spills at all time.

4.3. Start-up and Cool-down Procedure

In order to ensure accurate and reproducible results, a strict start-up and cool-down procedure has been put in place. The reason for this is twofold. Firstly, a lot of experiments conducted throughout this research have produced a cobalt salt precipitate. Without a strict procedure that ensures a proper flushing of all flow compartments, these contaminants might alter the outcomes future tests. Secondly, strict start-up and cool-down procedures are required to limit degradation of various components, such as ion exchange membranes and the diaphragms within the pumps.

Whilst a complete step-by-step guide for the start-up and cool-down procedures are eluded, as this would go beyond the objectives of this report, some important pitfalls are nonetheless highlighted. For instance, during the start-up procedure the various flow channels should be filled simultaneously, whilst the stack is maintained in the upright position. Doing so prevents unwanted ion and/or water transport through the various membranes. Furthermore, the stack should always be made clear of as much solid and liquid contaminant as possible before every experiment. Meaning, sufficient flushing of the stack with a salt solution should be performed before or after the bleeding of the stack.

Finally, it is paramount that the cell be filled with a salt solution, when left unattended for prolonged periods of time. This is necessary to prevent degradation of the membranes and the possible corrosion of the stainless steel fittings.

5

Experimental Results and Finding

The development of the solution to the hydrometallurgical drawbacks, discussed in this report, requires the realisation of a range of experiments, not all similar in nature. This is due to the fact that different experiments are set up for different reasons. Some experiments, encountered especially throughout the early testing phase, are developed in order to verify assumptions and thus require a rigorous scientific approach. Meaning that the outcomes of the experiments need to closely resemble previously established hypotheses. Other experiments, however, are conducted in order to generate new knowledge and, to some extent even, new ideas. In this case, experimental outcomes aren't known in advance and need to be set up through the use of another design philosophy, different from the one described earlier. In the course of this research, this category of experiments has been conducted through the use of a "trial and error" type method. Whereby quick experimental outcomes strongly motivate the possible pivoting to more appropriate setup configurations and, in some cases even, the utilization of other electrochemical techniques.

Moving on, it's worth mentioning that throughout the course of this research, the two experimental methods have not been used in sequence, but have rather been applied interchangeably. Which makes the development of a coherent and ordered display of the experiments conducted in this report challenging. Therefore, a successive display of the experiments has been avoided and the chapter is structured differently instead.

The chapter opens with a display of preliminary tests and results, which have, for the most part, been conducted in order to verify the predicted performance of both individual and integrated components. Simultaneously, the chapter presents a number of data analysis techniques used in later stages of the experimental part of this research.

The second part of this chapter explains a number of unforeseen issues encountered throughout the experimental phase of this research and presents various troubleshooting steps, utilized in order to achieve their respective resolutions.

The third subsection showcases the optimization steps, that have been conducted with the aim of achieving more efficient metal and acid recovery.

Finally, the fourth and final part of the chapter displays the results of the most successful experiment and examines the broader implications of it's outcomes.

5.1. Preliminary Tests and Results

The experimental setup, built for the purposes of this research, is complex in nature due the utilization of a large variety of technically advanced components. Examples of such components include ion exchange membranes, electrodes and toxic chemicals. Whilst correct predictions about both the indi-

vidual and integrated performance of these parts can be made, it remains crucial to verify its operation before proceeding to more complex experiments. Furthermore, conducting a variety of smaller experiments can lead to other benefits, such as a decrease in the probability for tedious and time-consuming troubleshooting steps in later stages of the research.

The subsection starts off with a display various experimental constraints. These include the limitations of the potentiostat, the limiting current density of the BPMs and the maximum achievable leaching efficiency of the metals from the LCO cathode material. Thereafter, the subsection displays a number of issues that have been identified during the early experiments. These include, for instance, the unforeseen oxidation of the cobalt ion within the metal recovery compartments and the negative effects of bubble formation during the start up procedure. The aim of this part of the report therefore, is to not just showcase results, but to highlight them as pivotal intermediate outcomes, that are responsible for a complete re-evaluation of the initial design configuration.

Finally, the latter part of this subsection explores the influence of a number of independent variables on important experimental outcomes. Examples of which, include the dependence of the acidity of the metal recovery compartment on different independent variables, such as the projected electrode areas or starting volumes of the electrolytic solutions.

Limiting Current Density
The experimental setup, as illustrated in figure 3.1, makes use of two bipolar exchange membranes in the forward bias mode. This implies that the membranes are operated in a configuration that promotes water dissociation on the boundary between the BPM's anion and cation exchange layers. In order for this dissociation to occur, a minimum theoretical potential of 0.86 V is required, which for commercially available BPMs corresponds to a current density of roughly 10 A/m2 [45]. This minimum amount of current is often referred to as the limiting current density and can be deduced experimentally from a current-voltage graph. In order to ensure proper operation of the BPMs, such an experiment has been realized. The set-up and results of which are displayed below.

Starting parameters

The independent variable in this experiment is the supplied voltage, which is swept from a value of 0 to 3.3 V. Meanwhile, the dependent variable for this experiment is the current density, the values of which are subsequently displayed in figure 5.1.

Table 5.1: Controlled Variables for the Current-Voltage Analysis

Controlled experimental parameters	Value
Projected electrode area	100 cm^2
Composition of the acid recovery, feed, metal recovery and rinse compartments	0.5 M NaCl
Flow rate in the acid recovery, feed, metal recovery and rinse compartments	48 ml/min

Results

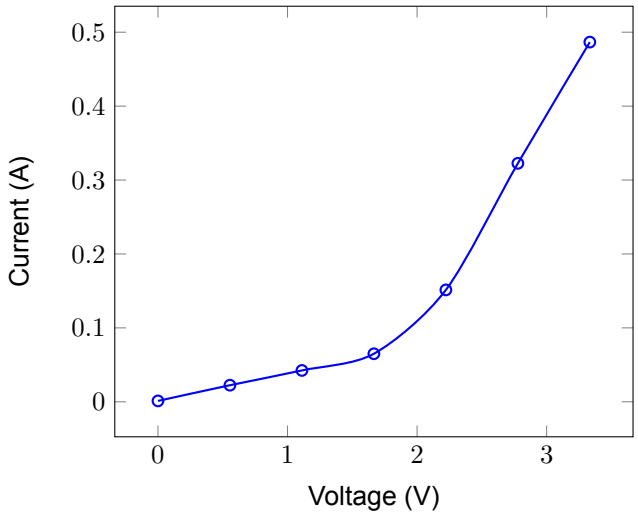

Figure 5.1: Voltage - Current profile for the experimental parameters displayed in table 5.1. The inflection point of this graph corresponds to the BPM's limiting current density

Below the limiting current density current is expected to be transported solely through the Na^+ and the Cl^- ions, present in the different compartment. Above the limiting current density, however, water dissociation is expected to take place, aiding the current transport through the BPMs. Figure 5.1 clearly displays this effect, as it showcases an inflection point at current of around 0.1 A. Noting that the projected electrode area in the experimental configuration equals 100 cm^2, the limiting current density is estimated to be around 10 A/m^2, which corresponds exactly with values found in literature.

Booster Limitations
Throughout the experimental part of this research, a maximum supply of 10 A at a potential difference of 30 V could be supplied to the setup by the potentiostat, when it coupled with the booster. As will be clarified later in section 5.2, most of the experiments conducted in this study need to be completed in a single, uninterrupted attempt, which creates the following challenge. Namely, If the voltage supplied to the stack isn't sufficiently high, then the time required for the metal ion diffusion to come to completion exceeds that of a workday. Since the laboratory environment, in which this study has been conducted, doesn't allow for unsupervised experiments to be performed overnight, this effectively implies that low voltage experiments could only be conducted to a partial extent.

In order to avoid this problem a majority of the experiments, realized throughout this study, are operated at the limit of the potentiostat, which has been determined preemptively through an experiment, displayed below.

Starting parameters

Table 5.2: Controlled variables for the booster limitation analysis

Controlled experimental parameters	Value
Projected electrode area	100 cm^2
Composition of the acid recovery, feed, metal recovery and rinse compartments	0.5 M NaCl
Flow rate in the acid recovery, feed, metal recovery and rinse compartments	48 ml/min

Table 5.3: Independent variable for the booster limitation analysis

Independent variable	Value in trial 1	Value in trial 2
Applied voltage	16 V	12 V

Results

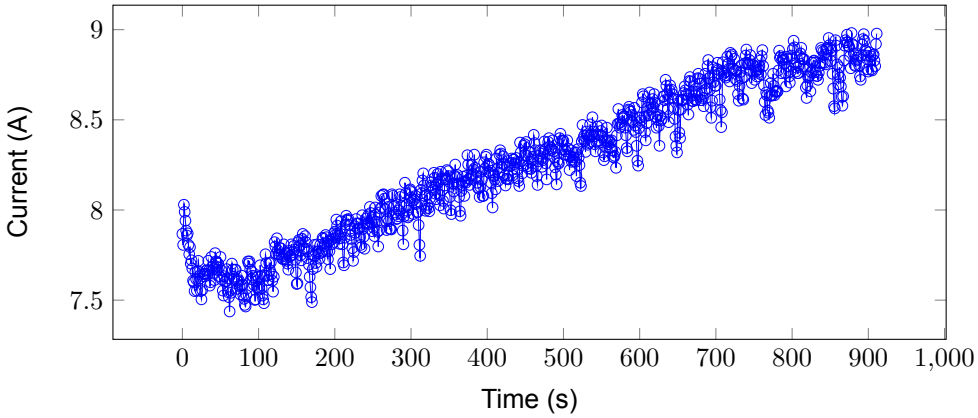

(a) Time-Current profile during an applied voltage of 16 V

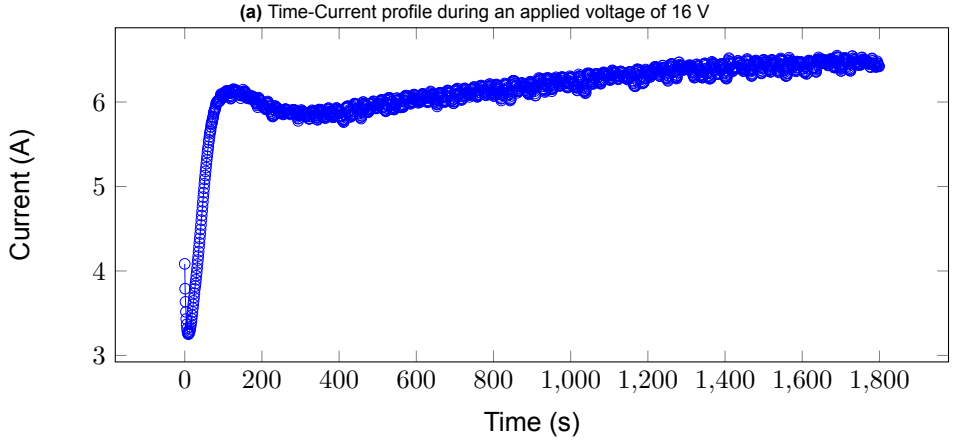

(b) Time-Current profile during an applied voltage of 12 V

Figure 5.2: Comparison of the time-current profiles for different supply voltages. The results were achieved through the use of the operational parameters mentioned in table 5.2.

Figure 5.2a displays the time-current profile for an applied voltage of 16 V. The gradient of this graph between 300 and 900 seconds is reasonably constant and amounts to 1 amp per 600 seconds. Had the experiment been continued for another 600 seconds and the gradient of the current-time graph would have remained constraint during this time, then a current of 10 A would have been reached. This causes a concern, since the booster utilized in this study is not designed to handle current above the 10 A limit. Therefore, in order to avoid this problem, the applied voltage throughout the course of this research has been lowered to a more appropriate value, like the one displayed in figure 5.2b.

Figure 5.2b displays the time-current profile for an applied voltage of 12 V. In the figure the gradient of the time-current graph flattens out at around 1800 s and the current reaches a maximum value of 6.5 A, which implies that prolonged operation of the setup at this configuration should remain well within the capacity of the booster.

The goal of this experiment was to determine a supply voltage that would ensure sufficiently fast metal ion diffusion rates, so that the experiments would come to completion within a work day. Whilst the

results for a supply voltage of 12 V, displayed in figure 5.2b, don't quite imply that the booster is being operated to its 10 A limit, this voltage has nevertheless been proven successful in achieving the metal recovery sufficiently fast throughout the remainder of this research.

Leaching efficiency
The leaching of cathode material is a well researched area within the hydrometallurgical recycling branch. Therefore, most of the optimal leaching conditions for various cathode structures can be found in literature. Matching these conditions, in the course of this research, has proven to be crucial, as it contributes to an accurate feasibility evaluation of the overall process in the final stages of this report.

As previously established in the literature review, nitric acid is a suitable leachant for the purposes of this research. In this section of the report, an experiment validating the effectiveness of the leaching conditions, as proposed in the works of Lee et al. and Pinna et al., is displayed and evaluated [44, 46].

Starting parameters

In order to properly assess the effectiveness of the leaching conditions provided by the works of Lee et al., the starting parameters and overall leaching setup should be replicated as closely as possible. However, the leaching setup in the works of Lee et al. is complex and difficult to reproduce, as it contains a number of additional components, such as a heater, stirrer and condenser [44].

For this experiment, therefore, the setup has been simplified. In doing so, the study notes another purpose for the conduction of this experiment. Namely, to confirm that the complexity of the setup, provided by Lee et al., is aimed at increasing the speed of the leaching process, rather than its overall efficiency.

Table 5.4: Starting parameters for the leaching experiment

Reactant	Concentation	Unit
LCO	20	g/L
HNO3	1	M
H_2O_2	1.7	% vol

Results

After 18 hours, the solution has been analysed using ICP-AES. The results of which, are displayed below in figure 5.5

Table 5.5: Results of the leaching experiment. The starting parameters of which are displayed in table 5.4

Reactant	Recorded leaching efficiency	Expected leaching efficiency from literature
Lithium	87 %	95 %
Cobalt	92 %	95 %

Table 5.5 shows that the experimental leaching efficiency slightly underperforms when compared to the efficiency achieved by Lee et al. [44]. However, this difference is small enough to confirm that the complexity in the Lee et al.'s. setup is aimed solely at increasing the speed of the leaching process and not the efficiency.

Moving on, the reason for the discrepancy in the expected and the recorded leaching efficiencies, shown in table 5.5 was not further investigated, as the recorded leaching efficiency is viewed as acceptable for the purposes of this research.

Nonetheless, some suggestions about this discrepancy can be made for future research anyway. One explanation for this discrepancy is the fact that Lee et al. used a closed container for the leaching pro-

cess, whereas the leaching solution in the context of this research was left exposed to air. This could potentially have influenced the oxidation rate of the cobalt ions.

Finally, this report underlines that the addition of hydrogen peroxide to the solution is crucial for the successful leaching of LCO material. This is likely to occur due to the reduction of Co^{3+} to Co^{2+}, as suggested by numerous authors, like, for example, Jung. et al. [14]. Throughout the course of this research, attempts have been made to leach the LCO material purely with nitric acid, all of which were unsuccessful.

Air Bubble Contamination: A Feasibility Calculation
Throughout the course of this research, the setup has made use of commercially available PTFE flow channels with fixed dimensions. The width of these channels, in unperturbed form, resembles the same order of magnitude as an air bubble, which poses a significant issue. Namely, that the surface tension effects of the air bubbles, potentially entrapped within the flowchannel mesh, could outweigh the bubble's buoyancy. If this happens, it would cause the bubbles to stick to the channel mesh, unless significantly fast flows are applied by pumps, more powerful than the ones utilized in this study.

A proof of this statement can be quickly achieved through some back of the envelope calculations, as is done next. To start, it is crucial to verify that the width of the flowchannel is indeed narrow enough to "hold" the bubbles in place. To do so, it is sufficient to prove that the height of the meniscus, formed on either side of the channel wall during the filling process, is larger than half of the width of the channel. This is done below through a scaling analysis.

Relevant parameters: γ,ρ,g,h

Whereby:

- γ - surface tension
- ρ - density of the liquid
- g - gravitational acceleration
- h - height of the meniscus

Dimensionless number π: $\sqrt{\frac{\rho g h^2}{\gamma}}$

Assuming π to be constant and substituting in values:

$$h = \sqrt{\frac{\gamma}{\rho g}} = \sqrt{\frac{0.072}{9.81 \times 1000}} = 2.7mm$$

$$h \geq \frac{1}{2} \times w$$

Whereby:

- w - width of the flow channel

$$2.7mm \geq \frac{1}{2} \times 1mm$$

This confirms, that the height of the meniscus is indeed larger than half of the width of the flow channel, which is about 1 mm. Proving, that the bubbles are indeed wide enough to be "stuck" to both sides of the flow channel.

Furthermore, in the conducted scaling analysis the walls of the flowchannel were modelled as solid. That is, without any cutouts in the mesh. To verify whether or not this assumption is valid, the Bond number (Bo) can be used, which describes the ratio between the gravitational and the surface tension force. In practice, a Bond number of below 1 would suggest, that if liquid was to be placed on the mesh in a horizontal position, then the it would fail to to penetrate the mesh. In turn, this would essentially confirm that the solid wall assumption is applicable.

$$Bo = \frac{gravitational force}{surface tension force} = \frac{\rho g}{\gamma / R^2} = \frac{\rho R^2 g}{\gamma}$$

Whereby:

- R - radius of the mesh gap

$$Bo \simeq \frac{1000 \times (1 \times 10^{-3})^2 \times 9.81}{0.072} = 0.138$$

The Bond number, calculated above confirms that the surface tension stress indeed outweighs the gravitationally induced stress, proving the validity of the assumption.

Next, it is important to verify that the buoyancy effects of the bubbles aren't sufficient to overcome the surface tension effects. To do so, a bubble is modeled as a cylinder, placed horizontally within the flow channel, as displayed in figure 5.3. Next, a force balance is conducted across the control volume displayed in blue.

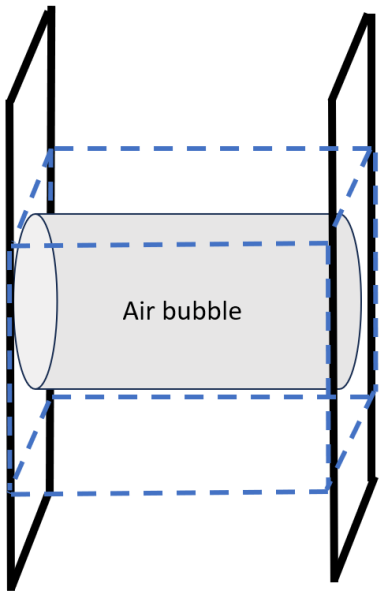

Figure 5.3: Sketch of the cross section of a flow compartment. The air bubble is displayed as a light-gray cylindrical shape. The control volume, utilized for an estimation of the bubble's buoyancy, is drawn around the bubble in the form of a blue rectangle.

$$F_{buoyancy} = F_{bottom} + F_{top} - F_g$$

Whereby:

- F_{bottom} - the force exerted by the water on the the bottom face of the control volume normal
- $Ftop$ - the force exerted by the water on the top face of the control volume
- F_g - weight of the control volume

$$F_{buoyancy} = \rho_w g \Delta h A - (V_b \rho_b + V_w \rho_w) g$$

Whereby:

- h - height of the control volume
- A - area of a single face of the cubical control volume
- ρ_w - density of water
- ρ_b - density of air
- V_w - volume of the water within the control volume
- V_b - volume of the air bubble

After further expansion of the formula above and substitution of numerical values the buoyancy is calculated to be in the order of 10^{-5} N.

Finally, the order of magnitude of the surface tension effects is estimated through the following back of the envelope calculation.

$$F_{st} \simeq \gamma \mathcal{P}$$

Whereby:

- F_{st} - downwards force on the bubble due to surface tension effects
- $\mathcal{P}$ - perimeter of the contact area between the bubble and the flow channel

After numerical substitution, F_{st} is estimated to be in the order of 10^{-3}, which is larger than the estimated value for the bubble's buoyancy. Meaning, that the presumption of bubbles remaining in the stack during operation is feasible.

Ultimately, this result implies that at any given moment the exact volume of the liquid solutions within the various flow compartments is unknown, leading to increased uncertainty of various experimental outcomes.

Visualization of Air Bubble Contamination Effects
During the operation of the stack, hydrogen is produced at the cathode, whilst oxygen is produced at the anode. As this happens, a part of these gasses remains ”stuck” within the flow channels, as previously established. Furthermore, throughout the course of this research it has been observed on a number of occasions that air can enters the four different flow compartments through improper sealing of the pump heads, adding to the accumulation gas.

During this accumulation a small part of the flow channel solutions get pushed out of the stack. In turn, this increases the volume of the solutions in the beakers, to which the flow compartments are connected. This poses an issue, since the volumes of these solutions are later utilized in mass balance calculations, which are used to determine the overall effectiveness of the design.
In this section, a visualization of the bubble accumulation is given. This is done through the conduction of an experiment, whereby the sum of the volumes within the different flow compartments is monitored for a prolonged operation of the stack.

Starting parameters

In this experiment the cell is operated in a manner that is similar to its operation during the actual metal recovery runs. The parameters of which are summarized below in table 5.6. Importantly, throughout this test 4 milliliter samples are taken from each beaker at various time intervals, which, in turn, are required for a separate analysis that is independent of this experiment. Because of this, the sum of the volume within the beakers is expected to decrease with time.

Table 5.6: Experimental parameters for the bubble contamination experiment. This experiment is set up in order to quantify the maximum bubble accumulation within the stack and is frequently referred to in subsequent uncertainty analyses.

Experimental parameters	Value
Projected electrode area	100 cm^2
Applied voltage	12 V
Initial total volume	1400 ml
Flow rate in acid recovery, feed and metal product compartment	48 ml/min
Flow rate in electrode rinse compartment	100 ml/min
Starting composition of feed compartment	1M HNO_3, 1.7 %vol H_2O_2, 1 g/L LCO
Starting composition and volume of product compartment	300 ml of 0.5 M NaCl solution
Starting composition and volume of acid recovery compartment	300 ml of 0.5 M NaCl solution
Starting composition and volume of electrode rinse compartment	500 ml 0.25 M Na_2SO_4 solution

In the experiment the volumetric sums are recorded in two steps. Firstly, the volume within the beakers is measured. Secondly, a fixed value of the total volume of the space within the tubes and the electrodialytic compartments is added. Since this added term may contain both liquids, as well as a significant portion of gas, generated at the electrodes or supplied to the stack by faulty pump heads, the actual measurement of total volume is expected to differ from the recorded value.

Results

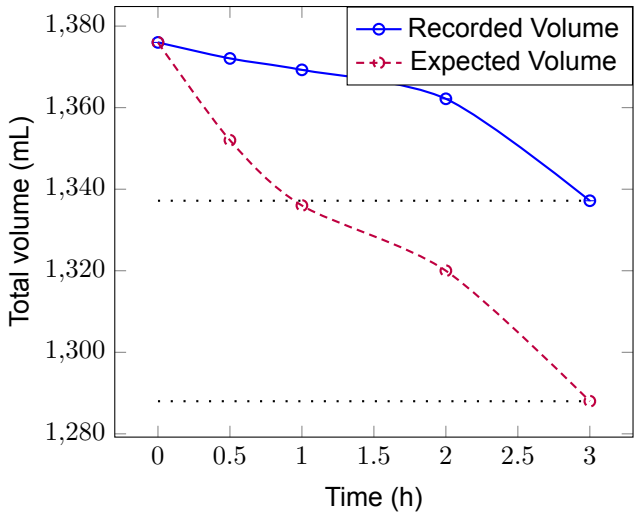

Figure 5.4: Visualization of the gas bubble contamination within the stack during operation. The starting parameters for this experiment are displayed in table 5.6. The blue plot represents the recorded volume of the sum of the electrodialytic solutions, which include the effects of the bubble contamination. The dotted red plot represents the expected sum of the solutions in case there is no contamination. The difference between these plots is used to quantify the total volume of gas accumulated within the stack during operation.

Figure 5.4 displays the outcomes of the experiment. In it, the red plot represents the expected sum of the volumes, contained within the different beakers, flow compartment and tubing.

At time = 0 h, this plot represents the total volume, immediately after the cell has been filled. If no air bubbles, “stuck” between the flow compartment walls would exit the stack over time, then this volume would remain constant. Or, to be more precise, decrease only due to the fact, that samples have been taken from the beakers at different time intervals. This explains why the expected volume in figure 5.4

decreases in time, instead of remaining constant.

The blue plot in figure 5.4, shows the physically recorded sum of the volumes. As displayed, this plot doesn't exactly follow the expected values. Instead, it deviates from the expected plot by a maximum of 50 milliliters at the timestamp of 3 hours. Since the meshed part of the flow channels of the electrode rinse compartment contains a total of 110 milliliters, this result effectively implies, that after 3 hours 45 percent of the meshed flow channel parts are occupied with gas bubbles.

Finally, it is noted that throughout the course of this research the difference between the expected and the recorded sum of the liquids contained within the beakers has never exceeded 50 milliliters. Therefore, for all subsequent analyses this value is taken as an upper bound for the uncertainty in the recorded volume of the electrode rinse compartment.

Volumetric Changes During Operation
Throughout the cell's operation ions get redistributed within the various electrodialytic compartments. As a result of this, the chemical potential of the different solutions change continuously, which, in turn, act as a driving force for a redistribution of solvent between the electrodialytic chambers. Furthermore, the volumes within the compartments throughout operation of the stack can be significantly influenced by the differences in electrochemical drag coefficients for the different ions. In order to display how the volumes within the various compartments change during operation the following experiment has been set up.

Starting parameters

The starting parameters for the visualization experiment are displayed below in table 5.6 and are reasonably representative of the starting parameters for the optimized mode of operation for the stack.

Crucially, it must explicitly be stated that the purpose for the conduction of this experiment is in actuality twofold. In the first place, the experiment is conducted for the purpose of visualizing the chemical potential effects, the results of which are displayed in this section. In the second place, the experiment is conducted in order to analyze metal recovery at a voltage supply of 12 volts, the results of which are discussed at a later point in section 5.3. Unfortunately, this second purpose demands the removal of samples from the various electrolytic compartments during the experiment, which significantly complicates a clear representation of the volumetric changes.

Table 5.7: Experimental parameters for the visualization of the solvent redistribution during operation.

Experimental parameters	Value
Projected electrode area	50 cm^2
Applied voltage	12 V
Initial total volume	1400 ml
Flow rate in acid recovery, feed and metal product compartment	48 ml/min
Flow rate in electrode rinse compartment	100 ml/min
Starting composition of feed compartment	1M HNO_3, 1.7 %vol H_2O_2, 1 g/L LCO
Starting composition and volume of product compartment	300 ml of 0.5 M NaCl solution
Starting composition and volume of acid recovery compartment	300 ml of 0.5 M NaCl solution
Starting composition and volume of electrode rinse compartment	500 ml 0.25 M Na_2SO_4 solution

Results

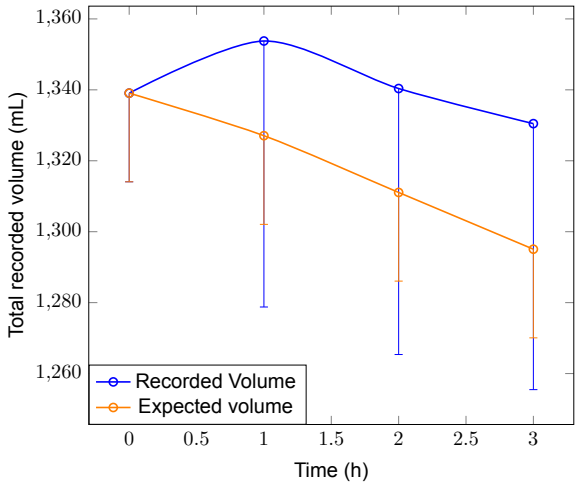

Figure 5.5: Visualization of the changes in the recorded volume during operation. The blue plot represents the recorded sum of the electrodialytic solutions, which include the effects of gas contamination. The orange plot represents the expected sum of the solutions in case there is no contamination present. The orange plot decreases with time due to the fact that samples are taken from the different solutions throughout the experiment.

Figure 5.5 displays the recorded volume of the sums of the solutions within the various electrodialytic compartments. To clarify, these sums account for the total volume of the liquids consumed in the experiment. Meaning, that they take into account a total of the solutions within the beakers, the stack and the tubing.

The sums are recorded in two steps. Firstly, the volume within the beakers is measured. Secondly, a fixed value for the total volume of the space within the tubes and the electrodialytic compartments is added. This added term may contain both liquids, as well as a significant portion of gas, generated at the electrodes or supplied to the stack by faulty pump heads, which makes the exact measurement of the volume within a certain compartment a challenge. To be specific, when air bubbles contaminate the stack a significant portion of liquid is forced out of the stack into the beakers, which consequently leads to measurements that are above the actual value for the volume contained within a specific compartment.

Finally, the orange line in figure 5.5 accounts for the fact that samples are removed from the different compartments throughout the course of the experiment and represents a calculated estimate of the true total volumetric sum.

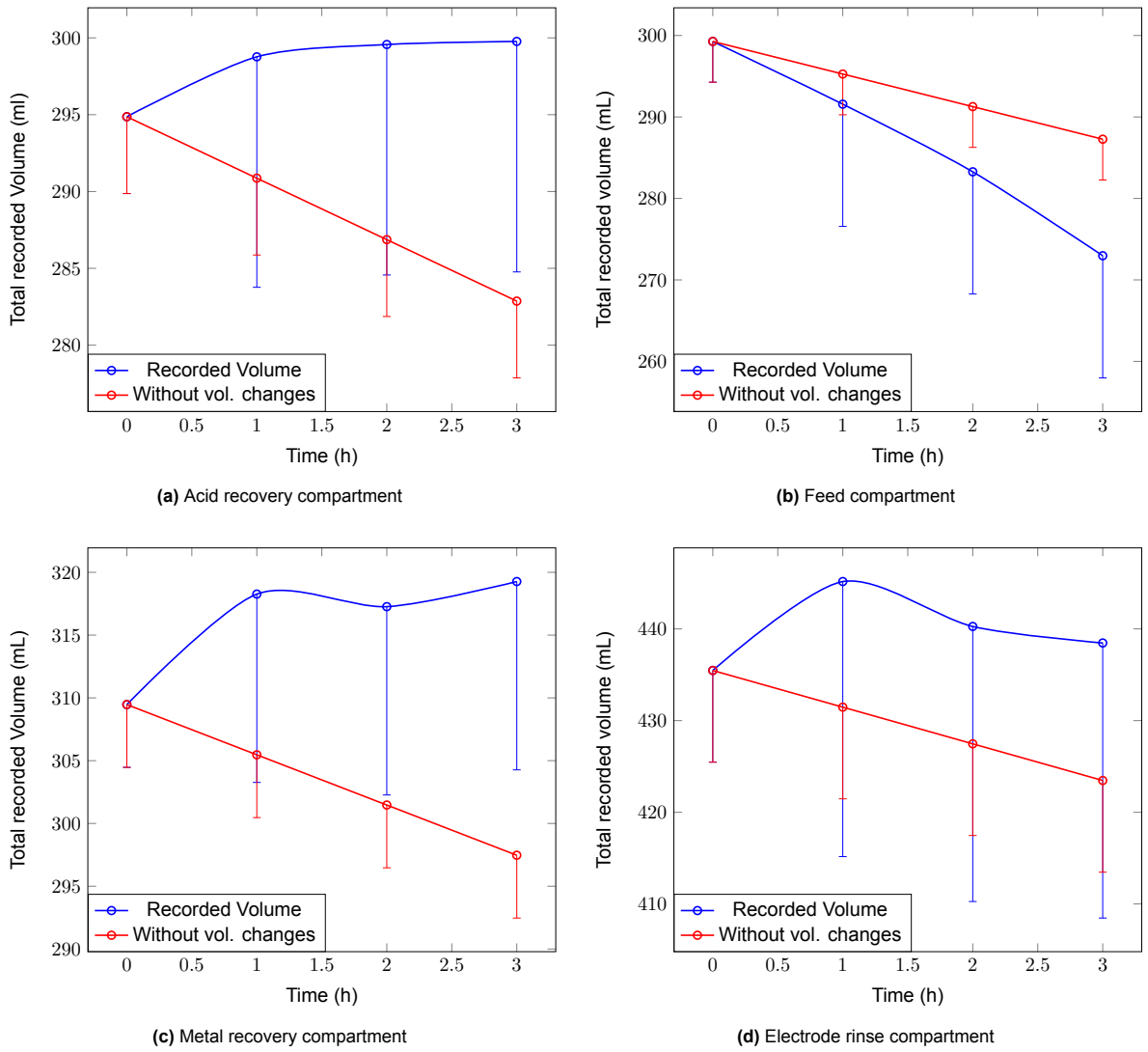

(a) Acid recovery compartment

(b) Feed compartment

(c) Metal recovery compartment

(d) Electrode rinse compartment

Figure 5.6: Volume changes in various electrodialytic compartments during operation. The starting parameters for this experiment are displayed in table 5.7. The blue plots represent the recorded volume of the solutions within the elctrodialytic compartments. The error bars of the blue plots account for the uncertainty generated by the stack's gas contamination. The red lines showcase the predicted volume of the solutions in case no solvent is redistributed during the experiment.

Figure 5.6 displays the volume changes of the solutions within the four different electrolytic compartments. In these figures, the red lines represent expected volumes of the solutions in the fictitious case that no solvent transport between the compartments takes place. In addition, the decreasing trend of the red lines is purely a result of the fact that samples are removed from the beakers at different points throughout the experiment.

Meanwhile, the blue lines in figure 5.6 represent the physically recorded volumes. Importantly, the blue plots in figures 5.6a and 5.6a extend above the red ones, which implies that the volume of the solution within the acid recovery and metal product compartments increase during operation of the stack. Meanwhile the opposite effect is observed in figure 5.6b.

The trends in the volume changes can be clarified in the following manner. During operation of the stack, ions within the feed compartment get depleted. To be specific, anions shift from the feed compartment to the acid recovery compartment, whilst cations move to the metal product compartment. Subsequently, through a combination of effects from electro-osmotic drag coefficients and changes in chemical potential differences part of the feed solvent gets depleted into its neighboring electrodialytic chambers.

Visualisation of Donnan Dialysis
The aim of this section is to display the Donnan Dialysis effects between the feed and metal recovery compartments. Ideally, these effects would be portrayed as a result of a distinct experiment, which would resemble the predicted outcomes of the diffusion displayed in figure 3.2. In order to achieve these results, however, the experimental design should be simplified to a configuration with fewer flow compartments and/or fewer ionic species. Otherwise, confusion would arise about the direction and magnitude of these migrations.

However, due to time constraints, the conduction of an experiment with a simplified design configuration is eluded. Instead, this report provides an admittedly weak visualization of Donnan Dialysis effects, that are inferred from changes in concentration within the compartments of the more complex setup. Furthermore, the visualization is complicated by the fact that this research has failed to set up an experiment with logical starting parameters. Due to the ever-present time constraints, this report utilizes the outcomes of a more important experiment, that has been allowed to come to completion, as the starting parameters for the visualization of the Donnan Dialysis instead.

For the purpose of coherence, some relevant starting parameters of the experiment that has been conducted first are displayed below in table 5.8. The other starting parameters, however, should be inferred from the results displayed by the first timestamp in figure 5.8, which showcases the complete diffusion of ions throughout the cell the final experiment.

Starting parameters

Table 5.8: Experimental parameters for the visualization of the Donnan Dialysis effects.

Experimental parameters	Value
Projected electrode area	50 cm^2
Applied voltage	0 V
Flow rate in acid recovery, feed and metal product and electrode rinse compartment	0 ml/min
Starting composition and volume of feed compartment	300 ml of 1M HNO_3, 1.7 %vol H_2O_2
Starting composition and volume of product compartment	300 ml of 0.5 M NaCl solution
Starting composition and volume of acid recovery compartment	300 ml of 0.5 M NaCl solution
Starting composition and volume of electrode rinse compartment	500 ml 0.25 M Na_2SO_4 solution

Results

Figure 5.7 shows the concentration of the hydrogen and sodium ions within the feed and metal recovery compartments at different times. The metal product compartment in the figure displays a decrease of sodium ion and an increase of the hydrogen ion concentration. In order for the desired Donnan Dialysis to be observed, the opposite trend in concentration within the feed compartment should be presented, just like in figure 3.2. However, even though the concentration of the sodium ion in the feed compartment is shown to have decreased, the hydrogen concentration is shown to have slightly increased.

The reason for this, however, is unlikely to disprove desired Donnan Dialysis. Rather, this surprising result is a probable consequence of the cell's complex configuration. As showcased in figure 5.8, hydrogen ions could have diffused from the acidic to the feed compartment first through the AEM, before further diffusing into the metal product compartment through the CEM. Consequently, no decrease in hydrogen concentration within the feed compartment is observed.

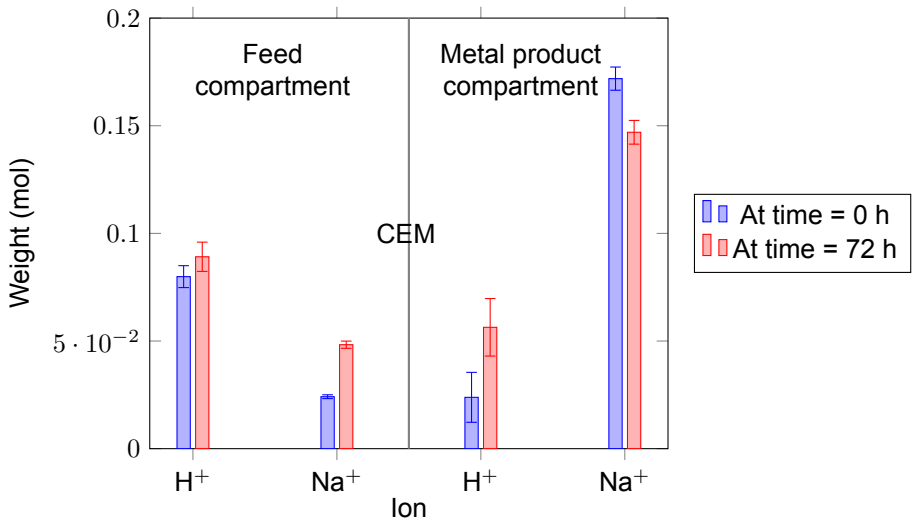

Figure 5.7: Visualization of the Donnan dialysis effects. The starting parameters for this experiment are displayed in table 5.8. The figure displayed a part of the BPMED setup, showcased fully in figure 3.1.

All in all, the results presented in figures 5.7 and 5.8 are likely to suggest that the pH within the metal product compartment can indeed be altered through Donnan Dialysis. However, more research is required in order draw robust conclusions about the rates, advantages and limitations of this technique.

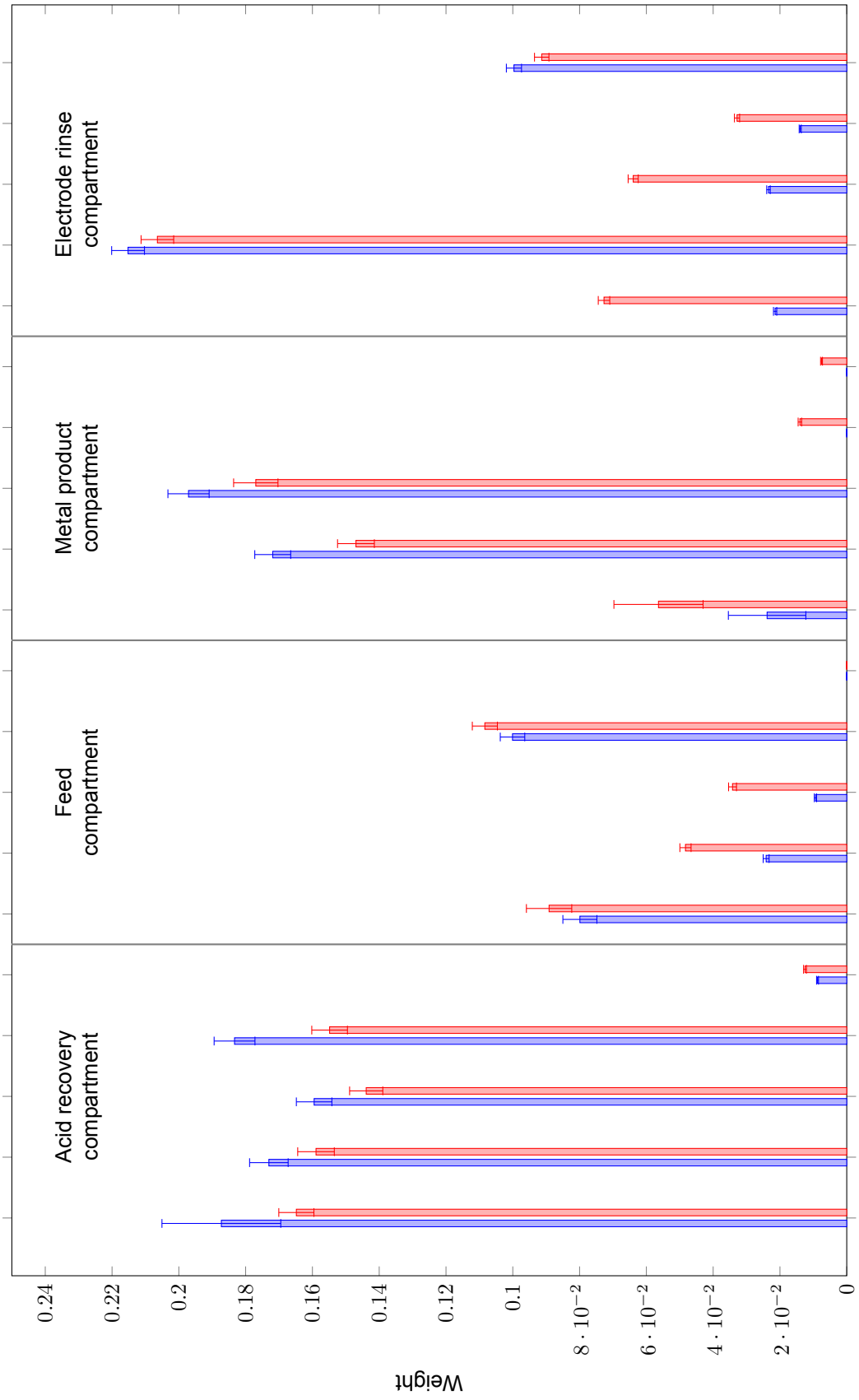

Figure 5.8: Full display of ions within the BPMED system for the visualization of Donnan (diffusion) Dialysis. The starting parameters for this experiment are displayed in table 5.7.

pH Measurement Techniques

An indirect goal of this research, eluded in the introductory chapter, is to maximize its overall scope within the time frame in which it is conducted. The performed experiments, therefore, are set up in a manner which allows for efficient, yet valuable data collection. One distinct way, in which the study achieves this, is through the use of elaborate, but automated data analysis techniques. An example of which is displayed in this section.

To a large extent, this study researches the influence of various parameters on the migration of ions in the context of BPMED. Subsequently, the study uses the acquired data for the purpose of establishing favorable parameters for lithium, cobalt and acid recovery from leached LCO cathode material in the BPMED system.

In order to analyze the migration of ions throughout the experimental part of this research, the use of ion-chromatography and mass-spectroscopy is required. To be precise, ion-chromatography is needed to determine the concentration of the NO_3^-, Cl^-, Na^+ and $SO4_2^-$ ions within the different electrodialytic compartments, whilst mass spectroscopy is required for the recording Co^{2+} and Li^+ concentration. Finally, pH measurements need to be conducted in order to determine the H^+ concentration. This step, as has been shown in practice, is time-consuming. Since the volume of the acquired test-samples is small, about 4 milliliters, the tip of the pH meter cannot be properly stirred in the sample. As a result, the time required for a substantial amount of H^+ ions to diffuse to the location of the pH meter's electrodes increases, forcing an accurate measurement to take about 8 minutes per sample.

Therefore, where possible, the H^+ concentration has been determined differently. Since the total concentration of all other ionic species present within the system are systematically acquired through ion-chromatography and mass-spectroscopy, the difference in the total number of positive to negative charges can be calculated and used to infer the H^+ concentration. This statement is a consequence of the law of electroneutrality, a proof of which is showcased in this section.

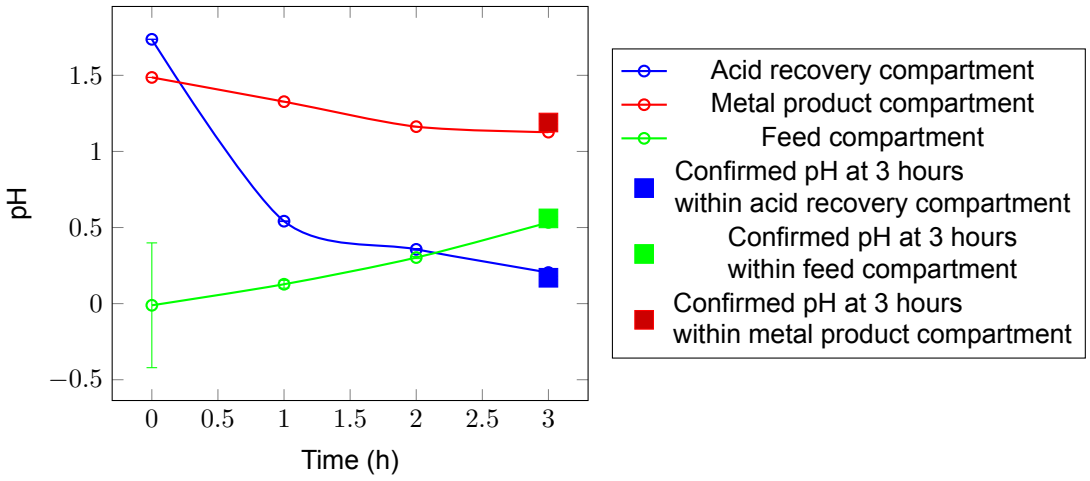

Figure 5.9: Verification of the analytical pH calculations. The lines represent the analytically determined pH values of the different electrodialytic solution during a particular experiment. The square points display the recorded pH values of the solutions through the use of a pH meter.

Figure 5.9 displays the recorded pH results of an experiment, the starting parameters of which are displayed in table 5.6, but the purpose of which is irrelevant for this section of the report. Here, only the effectiveness of the mentioned measurement technique for the hydrogen ion concentration (and hence also the pH) is of concern. In figure 5.9 the various graphs represent the measured pH of the various compartments through means of the analytical method. In turn, the squares in figure 5.9 display the physically recorded pH values by a pH meter.

As shown, the physically recorded measurements correspond well with the analytically predicted ones, implying that the chosen analytical method is indeed effective.

Finally, in figure 5.9 the error bar for the analytical pH measurement for the feed compartment at a time stamp of t = 0 is disproportionally large, when compared to the other errors in the figure. This error arises from the manner in which the pH is calculated and, consequently, the way in which the error propagates throughout this process. The step, which contributes most to this value the most, is the conversion of the H^+ concentration into it's respective pH value, as is explained in further detail below.

The starting point for the explanation the formula for the pH in terms of proton concentration.

$$pH = -\log(H^+)$$

Whereby:

- H^+ - refers to the proton concentration

Next, the uncertainty for the proton concentration is converted into the uncertainty for the pH through a Taylor expansion about the operation point.

$$u_{pH} = \left.\frac{d(pH)}{d(H^+)}\right|_{H^+=\bar{H}^+} \times u_{H^+}$$

Whereby:

- u_{pH} - uncertainty in pH
- u_{H^+} - uncertainty in H^+ concentration

$$u_{pH} = \frac{1}{\ln 10} \times \frac{1}{x}$$

Finally, the derived formula is able to clarify the error bars in figure 5.9, showing that the uncertainty in the pH increases with increasing proton concentration.

Precipitate Analysis
In chapter 3 one of the primary technological challenges of this research has been outlined. It stated that the electrodialytic system, built for the purposes of this thesis, must ensure the complete dissolution of metal ions in all of its compartments. In addition to this, the chapter implied that if a precipitate in the product compartment was to form anyways, it would likely take the form cobalt hydroxide. This hypothesis is significant, as solubility data for cobalt hydroxide can be extracted from scientific literature and used to determine favorable starting and operational parameters. The data that this research has relied on most is the work conducted by Gayer and Garrett [47].

However, throughout the early experimental phase a precipitate has been observed to form in spite of the data provided by Gayer and Garrett. As a result of this, X-ray diffraction had to be used in order to determine the exact composition of the precipitate. The process for which is seen as the main objective of this section.

Starting parameters

In order to produce a substantial amount of precipitate in the product compartment, a separate experiment has been set up. The starting parameters of which are displayed in table 5.9. Importantly, the starting composition of the feed solution for this experiment contains an increased amount of leached LCO material, which allows for more precipitation.

Table 5.9: Experimental parameters for the increased generation of cobalt precipitate.

Experimental parameters	Value
Projected electrode area	100 cm^2
Applied voltage	12 V
Flow rate in acid recovery, feed and metal product compartment	48 ml/min
Flow rate in electrode rinse compartment	100 ml/min
Starting composition of feed compartment	1M HNO_3, 1.7 %vol H_2O_2, 30 g/L LCO
Starting composition and volume of product compartment	300 ml of 0.5 M NaCl solution
Starting composition and volume of acid recovery compartment	300 ml of 0.5 M NaCl solution
Starting composition and volume of electrode rinse compartment	500 ml 0.25 M Na_2SO_4 solution

After sufficient precipitate is formed, the precipitate is filtered out from the product compartment and put forward towards the XRD measurements. Note, that the filtering process was complex and required various troubleshooting steps, which are explained later in the section 5.2.

Results

The precipitate was formed as a dark-brown paste and was deposited and dried on a Si510 zero-background wafer. Subsequently, the sample was analysed with the use of a Bruker D8 Advance diffractometer.

Table 5.10: XRD results for the precipitate, frequently found within the metal product compartment.

Compound name	Formula
Heterogenite-3R,syn	Co+3O(OH)
Cobalt Oxide	CoO_2

The composition of the X-ray diffraction results are displayed in table 5.10 and imply that cobalt oxide is formed within the metal product compartment instead of the predicted cobalt hydroxide. This result is significant, as it implies that the cobalt oxidises from $Co2^+$ to $Co3^+$ in the course of the experiments. Furthermore, since cobalt oxide is less soluble in acid than cobalt hydroxide this significantly reduces the effectiveness of the proposed solution.

5.2. Problem Resolution and Troubleshooting Methods

During the early testing phase of the experimental part of this research a number of flaws in the experimental design have been identified and categorized into two distinct categories. The issues that make up the first category are ones that have the potential to be solved directly through a simple troubleshooting solution. In the second category, however, are problems that are inherent to the initial design philosophy. A resolution of which would require a complete redesign of the overall setup.

The aim of this chapter, therefore, is also twofold. Firstly, the chapter illuminates various issues encountered during the experimental phase of this research and explains the changes made to the setup in order to achieve their resolution. Secondly, the chapter presents the flaws, which have proven to be inherent to the chosen design and cannot be solved directly. Here, the chapter shifts its focus to explore the various experimental bounds, within which the effects of these issues are minimized or bypassed completely.

XRD measurement complications
Throughout the course of this research a number XRD measurements had been conducted in order to establish the chemical composition of the formed solid precipitates, the most important result of which is displayed in section 5.1 under the header “Precipitate Analysis”. A successful execution of these measurements, however, has proven to be challenging due to a number of reasons. All of which, including their respective resolutions are clarified in this section.

In order to aid coherence, the solution to the measurement complication is structured in the following way. First and foremost, the report explicitly showcases the main issues that hinder a successful measurement. After that, various attempts aimed at their respective resolutions are discussed. Finally, the report presents the definitive process that leads to the desired outcome.

The confronted issues can be divided into three categories. The first category of issues stems from the fact that the fine solid precipitate needs to be collected onto a separate and appropriate background, like a silicon wafer. The second, from the fact that sufficient precipitate generation within the setup is limited by the diaphragm pumps, since these aren’t designed to handle multiphase liquid and solid flow. Finally, there are a number of solutions that are hindered by the fact that the precipitate needs to be collected in a reasonably pure form, without any salt contamination.

In the initial measurement attempts, the solid has been collected through the process of vacuum filtration, which leads to issues of the first category. To be specific, throughout the vacuum filtration process the cobalt precipitate seemingly intercalates with the filter paper, due to its fine nature. This makes the subsequent removal of the solid onto the wafer impossible. Therefore, the method of collection through vacuum filtration is abandoned, and a new approach is designed.

In the subsequent troubleshooting attempt, a mixture of the solid precipitate and its respective solvent is collected into a beaker and left untouched for 12 hours. During this time, the fine solid particles collect on the bottom of the beaker due to its higher density. After that, the solid particles (and some liquid) is removed from the bottom of the beaker using a pipet and deposited onto a silicon wafer. Next, the wafer is heated in order to evaporate the liquid, before the process is repeated. This method, however, has led to issues of the second category, meaning that the collected cobalt precipitate is contaminated with impurities to an extent, whereby an accurate measurement is no longer possible. An example of such a measurement is displayed below in table 5.11.

Table 5.11: Intermediate XRD results for the precipitate, often found within the metal product compartment. The accuracy of the results is limited by poor precipitate collection.

Compound name	Formula
Halite	NaCl
Sodium Cobalt Oxide	$Na_{0.34}CoO_2$
Cobalt Oxide	$CoO_{1.72}$

Finally, in order to solve the issue associated with the salt contamination, the following process has been designed. Namely, after removal of the solid precipitate (and some liquid) from the bottom of the beaker using a pipet, the mixture is placed into a test tube, suitable for a centrifuge. Next, the mixture ran through the centrifuge, which forces the precipitate to firmly stick to the bottom of the tube. This hence allows the removal of the liquid in order for it to be replaced with demineralised water. If the centrifuge process is subsequently repeated, the salt contaminants are dissolved into the new solvent, thus purifying the problematic cobalt precipitate. This method of solid collection has proven to work well and has lead to the successful results displayed earlier in table 5.10.

Leakage Analysis
The first experiments, conducted in this study, suffered from a consistent leakage problem. To be specific, the solutions contained within the metal product and the electrode rinse compartment mixed together after prolonged operation of the stack. Therefore, this section of the report focuses on clarifying the exact issue in combination with its respective resolution.

The structure of this section consists of three parts. Firstly, a number of ineffective troubleshooting methods are showcased. Secondly, the origin of the leakage problem itself is reevaluated, through the conduction of an important back-of-the envelope estimation. Finally, the report explores two applicable solutions to the issue, yet clarifies that these solutions have a similar respective drawback.

Preliminary troubleshooting attempts

The initial troubleshooting attempts were conducted under the assumption that the leakage arose from a failure in the BPM between the metal product and electrode rinse compartments. In the very first try to resolve this, the BPM was simply removed from the stack and replaced with a fresh one. This, however, solved the issue for a short period of time only.

The next troubleshooting attempt entailed a replacement of the BPM once again, but contained an additional exchange of the utilized salt within the electrode rinse compartment from NaCl to Na_2SO_4. The reason for which, stems from the fact that chlorine gas can be harmful to BPMs. And, since the issue occurred at the cathode side of the stack, where chlorine ions could potentially be reduced to chlorine gas, the exchange of salts seemed like a plausible solution. Which, in the end, didn't resolve the leak.

Identification of gasket failure

After these initial troubleshooting attempts, the focus shifts from the realization of the troubleshooting ideas to an in-depth investigation of the leak itself. Hereby, the stack is reviewed with increased caution and, as a result, an observation is made about the state of the gaskets within the stack. Namely, it is noticed that the EPDM gaskets surrounding the BPM look different from the others and contain traces of thermal-like induced damage. A representation of which is displayed below in figure 5.10.

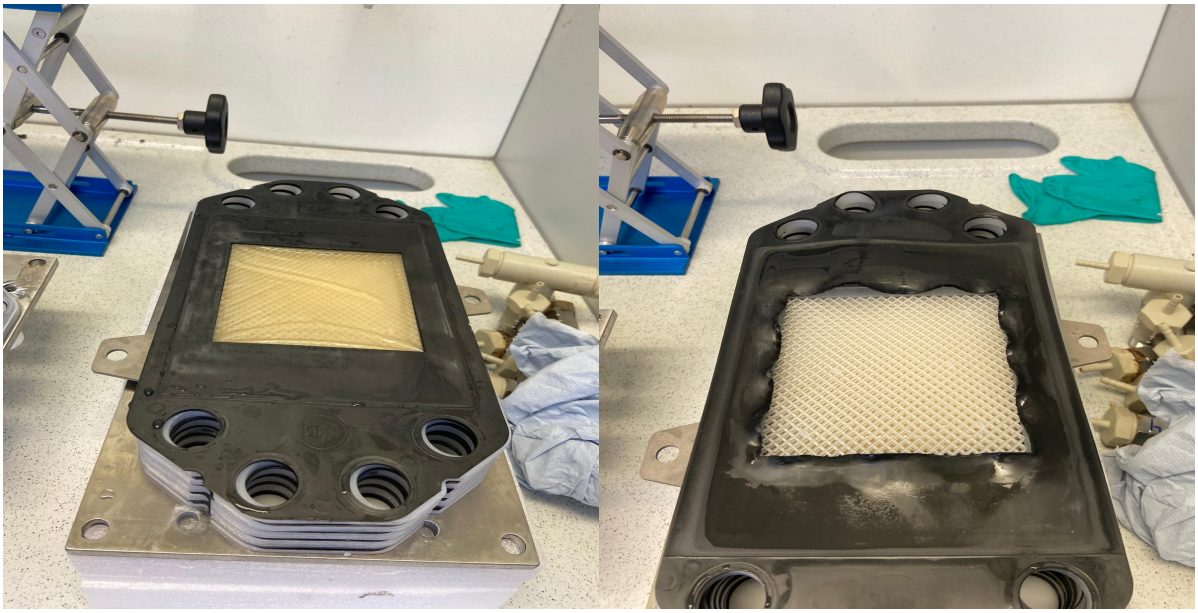

(a) Unperturbed gasket **(b)** Broken gasket

Figure 5.10: Display of working and broken EPDM gaskets

Figure 5.10a displays a healthy gasket, whilst figure 5.10b shows one of the damaged ones. In figure 5.10a the center cutout of the gasket is perceived as completely intact. Its edges seem to be flat and stick properly to the ion exchange membrane below it. The cutout in figure 5.10b, however, displays a wave-like profile and hence, implies signs of acquired heat or pressure damage. Regardless of the exact nature of the failure, at this stage of the research the gasket failure is identified as the most prob-

able cause of leak between the electrode rinse and metal product compartment. Subsequently, the origin of the gasket failure itself requires investigated, as is done in the next.

Origin of Gasket Failure

In section 5.1 under the header ”Air bubble contamination: a feasibility analysis” the feasibility of bubble accumulation within the different flow channels has been investigated and confirmed. Importantly, section 5.1 proved through a back-of-the envelope calculation that the surface tension effects of the bubbles are in roughly the same order of magnitude of the bubbles' buoyancy effects. Meaning, that without significant liquid flow rates through the flow channels, these bubbles may remain within the stack and cause a pressure build up. This theory is further supported by the location of the gasket failure. Namely, close to the cathode, where the hydrogen evolution reaction occurs. Which, in the case of this design configuration, produces the most gas by volume.

Theory validation

In order to confirm the theory fully the following feasibility analysis is conducted. Within it, the volumetric hydrogen production rate is compared to the volumetric flow rate through the electrode rinse compartment. Whereby, similar orders of magnitude would effectively verify the validity of the hypothesis.

The first step of the feasibility analysis notes that throughout the majority of experiments conducted within this research, the electrode rinse compartment maintained a slightly alkaline condition. Therefore, the following equations for the reactions at the electrodes displayed below.

$$4OH^- = O_2 + 2H_2O + 4e^- \tag{5.1a}$$

$$4H_2O + 4e^- = 2H_2 + 4OH^- \tag{5.1b}$$

Next, it is noted through reaction 5.1b that 1 mol of hydrogen gas is produced per 2 electrons supplied by the potentiostat. Subsequently, it is possible to deduce the number of hydrogen moles produced at the cathode per unit of time by converting the current supplied to the stack into the number of electrons per unit of time.

$$\textit{Step 1:} \quad I\left[\frac{e}{s}\right] = \frac{1}{1.6 \times 10^{-19}} \times I\left[\frac{C}{s}\right]$$

Whereby:

- I - current
- e - unit of elementary charge, amounting to $1.6 \times 10^{-}19$ Coulombs

$$\textit{Step 2:} \quad \dot{H}_2\left[\frac{mol}{s}\right] = \frac{I\left[\frac{e}{s}\right]}{2N_a\left[\frac{1}{mol}\right]}$$

Whereby:

- $\dot{H}_2$ - hydrogen production rate
- N_a - Avogardo's constant, amounting to 6.022×10^{23} particles per mole

$$\textit{Step 3:} \quad \dot{H}_2\left[\frac{mL}{s}\right] = 22.4\left[\frac{L}{mol}\right] \times 10^3 \times \left[\frac{mL}{L}\right] \times \dot{H}_2\left[\frac{mol}{s}\right]$$

After the substitution of values into the above equations, the maximum time required in order for the problem flow compartment is found to be around 30 seconds. In the meantime, the time required for the pumps to refresh the solution within the same compartment is found to be in the same order of magnitude, 25 seconds. Implying, that the bubbles are indeed likely to remain stuck within the chamber's mesh, causing a pressure build-up and the subsequent gasket failure.

5.3. Design Optimization

In previous sections of this chapter the preliminary tests and results, and the various troubleshooting methods have been displayed. As a result of which, a working design has been developed within a specific range of operational parameters. In this section of the report, the research further improves this setup through investigating the effects of different variables on the desired outcomes.

This process, as will be clarified later, is complex in nature for a number of reasons. Firstly, the design setup is in itself quite complex due to the presence of multiple compartments, each containing different solutions. By optimizing one parameter, therefore, another might be worsened. Secondly, the optimization steps are complicated by the physical scale of the BPMED setup. Due to its size, the time it takes for an experiment to come to completion is reasonably large, which consequently lowers the total number of experiments that can be conducted within the timeframe of this study.

Next to a display of the optimization steps, therefore, this section focuses on a clarification of the motivation behind the strict selection of the conducted experiments and the ranges for the optimized parameters.

Volume influence on acidity

One of the main research objectives of the experimental phase of this research is the minimization of the pH within the metal product compartment. By achieving this the potential number of cobalt ions in dissolved form within the compartment is increased, which ultimately leads to an improved recovery efficiency.

In an initial attempt to optimize this, the influence of the starting volumetric ratio between the feed and metal product solution on the acidity of the solutions within the different compartments is investigated.

Starting parameters

In order to ensure that the experimental outcomes are a direct consequence of the change in the volumetric starting ratio all other experimental variables are, where possible, controlled and displayed in table 5.12.

Table 5.12: Controlled variables for the optimization of the feed to metal product solution ratio.

Controlled variable	Value
Applied voltage	12 V
Projected electrode area	100 cm^2
Flow rate in all compartments	48 ml/min
Starting composition of feed compartment	1M HNO_3, 1.7 %vol H_2O_2
Starting composition and volume of product compartment	300 ml of 0.5 M NaCl solution
Starting composition and volume of acid recovery compartment	300 ml of 0.5 M NaCl solution
Starting composition and volume of electrode rinse compartment	400 ml 0.5 M NaCl solution

In order to conclude if the volumetric ratio has an effect on the acidity within the metal product compartment efficiently, a significantly large difference in the independent variables is chosen, as displayed in table 5.13.

Table 5.13: Independent variable for the optimization of the feed to metal product solution ratio.

Independent variable	Value in first trial	Value in second trial
Ratio between the feed and the product compartment	1:1 (300 ml : 300 ml)	5:1 (1500 ml : 300 ml)

Results

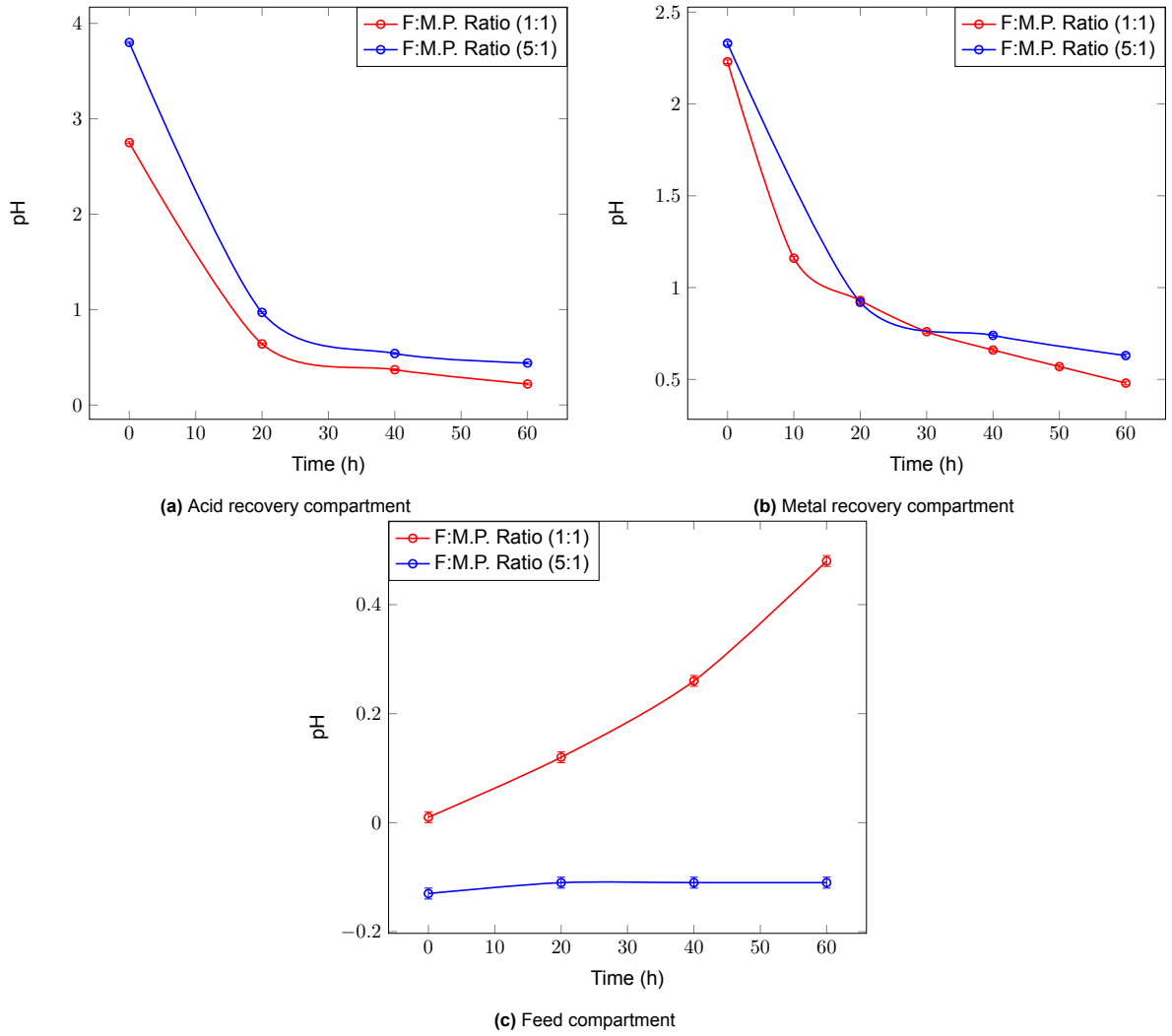

(a) Acid recovery compartment

(b) Metal recovery compartment

(c) Feed compartment

Figure 5.11: Visualization of the relationship between the feed to metal product volume ratio on the acidity of the different compartment solutions. The starting parameters for this experiment are showcased in tables 5.12 and 5.13.

The results of the conducted experiments are displayed above in figure 5.11. Interestingly, figures 5.11a and 5.11b showcase that the changes in the volumetric ratios barely influence the acidity of the acid recovery and metal product compartment respectively throughout the duration of the experiment.

In an attempt to clarify this outcome, the proton's molar flux through the CEM is expressed through the Nernst-Planck equation. Taking the model proposed by MacGillivray, which assumes the Nerst-Einstein relation and neglects the the contributions from bulk flow of water, relationship simplifies to the form displayed in equation 5.2 [48].

$$J_i = (\frac{D_i}{RT})Fc_i(\frac{d\phi}{dx}) - D_i(\frac{dc_i}{dx}) \tag{5.2}$$

Whereby:

- J_i - flux of the *i*th species
- D_i - diffusion coefficient of the *i*th species
- ϕ - electric potential

- F - Faraday's constant
- R - universal gas constant
- T - temperature

Next, the terms $\frac{d\phi}{dx}$ and $\frac{dc_i}{dx}$ are expanded to $\frac{\Delta\phi}{\mu}$ and $\frac{\Delta c}{\mu}$ respectively, whereby μ refers to the thicknes of the CEM. Next, since the membrane resistance is provided by the manufacturer, $\Delta\phi$ can be estimated through ohm's law. Finally, a subsequent substitution of appropriate values leads to an estimated value of the $\Delta\phi$ term of around 0.25 V.

Moving on, the magnitude of the two terms on the right side of equation 5.2 are compared. To do this, the equation is first rewritten into the form displayed below.

$$J_i = D_i[(\frac{1}{RT})Fc_i(\frac{\Delta\phi}{\mu})] - D_i[(\frac{\Delta c_i}{\mu})]$$

The order of magnitude of the terms displayed in the square brackets within the given equation can now be estimated. Through a substitution of the relevant parameters, the first term is estimated to be a factor 10 larger than the second. Meaning, that the dominant form of ion transport is due to the electro-osmosis.

By following the simplification of the Nernst-Planck relation as proposed by MacGillivray, the c_i term in the left part of equation 5.2 can be taken as the proton concentration within the feed compartment [48]. Looking at the data implied by figure 5.11, the proton concentration within the feed compartment changes by a factor of roughly 60 % within 60 minutes in a reasonably linear manner. If the average flux between the feed and metal product compartment is calculated at the average proton concentration within the feed compartment during the experiment, namely at the 30 % mark, a similar proton concentration increase should be observed within the metal product compartment, shown in figure 5.11. This however, doesn't happen.

Therefore, this research notes that the influence of the volumetric ratio between the feed and metal product compartment has little effect on the acidity of the product compartment. Simultaneously, this study underlines that more effort is required to explain this outcome. Or, perhaps, the experiments should be repeated in order to verify the reliability of the displayed results.

Supply voltage influence on metal transfer rate
In order for the lithium and cobalt ions to effectively penetrate the CEM between the feed and metal product compartments, a sufficiently large potential difference has to be applied to the stack. Therefore, the goal of this section is to investigate the minimum supply voltage required to achieve effective metal recovery. In addition to this, the supply voltage is expected to have a profound effect on the membrane's selectivity. Results of which are also analyzed from the experimental outcomes displayed in this section.

Starting parameters

Ideally, all the experimental parameters apart from the independent and dependent variables in this optimization step would be controlled. However, in lieu of time constraints, the potential number of experiments that can be completed within this study is limited, which forces some investigations into the dependence of experimental outcomes on different variables to be conducted simultaneously. As a result of this, the amount of the leached cathode material in this experiment could not be held constant, as shown in table 5.15. Nonetheless, the report notes that the values in table 5.15 are in the same order of magnitude, which indirectly implies that the experimental outcomes for the metal's respective recovery efficiencies should still be reliable.

Apart from the controlled variables stated in table 5.14, the starting composition of the feed compartment could have been controlled. However, due to the trial and error type of experimentation in the early stages of this research, the LCO solid to liquid ratio has been decreased.

Table 5.14: Controlled variables for the optimization of the supply voltage.

Controlled variable	Value
Projected electrode area	100 cm^2
Flow rate in all compartments	48 ml/min
Starting composition of feed compartment (not including LCO)	1M HNO_3, 1.7 %vol H_2O_2
Starting composition and volume of product compartment	300 ml of 0.5 M NaCl solution
Starting composition and volume of acid recovery compartment	300 ml of 0.5 M NaCl solution
Starting composition and volume of electrode rinse compartment	400 ml 0.5 M NaCl solution

Table 5.15: Other variables for the optimization of the supply voltage.

Other variables	Value in trial 1	Value in trial 2
Starting LCO concentration in feed compartment	12 g/L	3.3 g/L

Table 5.16: Independent variable for the optimization of the supply voltage.

Independent variable	Value in trial 1	Value in trial 2
Applied voltage	6 V	12 V

Results

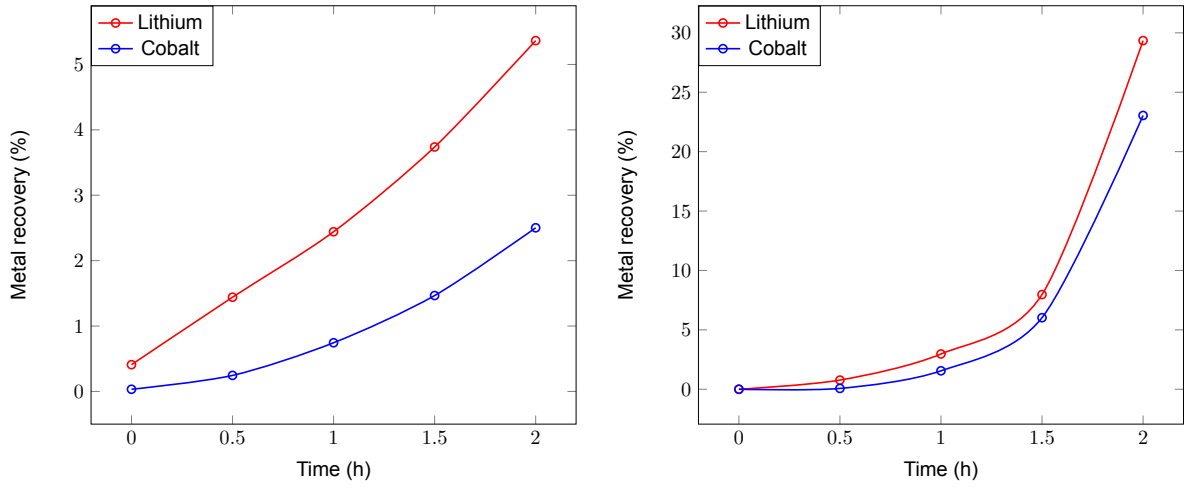

(a) Metal recovery at 6V

(b) Metal recovery at 12V

Figure 5.12: Metal recovery changes due to variations in the supply votlage. The starting parameters for the this experiment are displayed in tables 5.14, 5.15 and 5.16.

Figures 5.12a and 5.12b display the metal recovery percentages for lithium and cobalt for a supply voltage of 6 and 12 volts respectively.

Firstly, it is observed that the lithium recovery at 12 V is significantly higher than at 6 V. Whilst it may be concluded that a higher voltage leads to faster recovery, definitive statements about the absolute numeric increase should be eluded due to the fact that the starting LCO concentration in the feed has not been controlled in this experiment.

Secondly, it is noted that the selectivity changes with an increase in the applied potential difference, which could be the result of a number of factors. For instance, this outcome could be a consequence of the fact that the electronegativity of cobalt is higher than that of lithium. Meaning, that a higher applied voltage is required to separate the ion from its nitrate and subsequently force it through the CEM. Alternatively, the selectivity change could be a result of the fact that the cobalt ion is more positively charged. Which implies that in order for the electroneutrality to be conserved within the metal product

compartment more monovalent cations need to be pushed out, or more hydroxide ions need to be supplied to the compartment by the BPM. Finally, the result could also stem from the fact that the depletion of the protons from the feed compartments is more rapid at 12 V, which ”frees up” space for other ions, such as the lithium and cobalt to be transported

Pulsating Current Influence on Acidity
In section 5.2 under the header “Gasket Failure” an important issue surrounding the excessive gas generation at the electrodes has been investigated. This section, in turn, presents an attempt at the problem’s respective resolution.

To be specific, this section aims to investigate whether shifting the supply voltage, applied to the cell, from constant to pulsating could resolve the issue. The frequency of the pulsation is chosen in a way that would allow for sufficient time for the bubbles to be removed from the stack, before the voltage is turned on again. The full estimation of which is provided in the appendix.

Table 5.17: Controlled variables for pulsating current solution.

Controlled variable	Value
Applied voltage	12 V
Projected electrode area	100 cm^2
Flow rate in all compartments	48 ml/min
Starting composition of feed compartment	1M HNO_3, 1.7 %vol H_2O_2
Starting composition and volume of product compartment	300 ml of 0.5 M NaCl solution
Starting composition and volume of acid recovery compartment	300 ml of 0.5 M NaCl solution
Starting composition and volume of electrode rinse compartment	400 ml 0.5 M NaCl solution

The controlled variables for the two conducted experiments are displayed in table 5.17. The independent variable, the supplied voltage, is altered from constant in the first trial pulsating in the second, whereby the supply voltage is switched on and off every 15 seconds.

Results

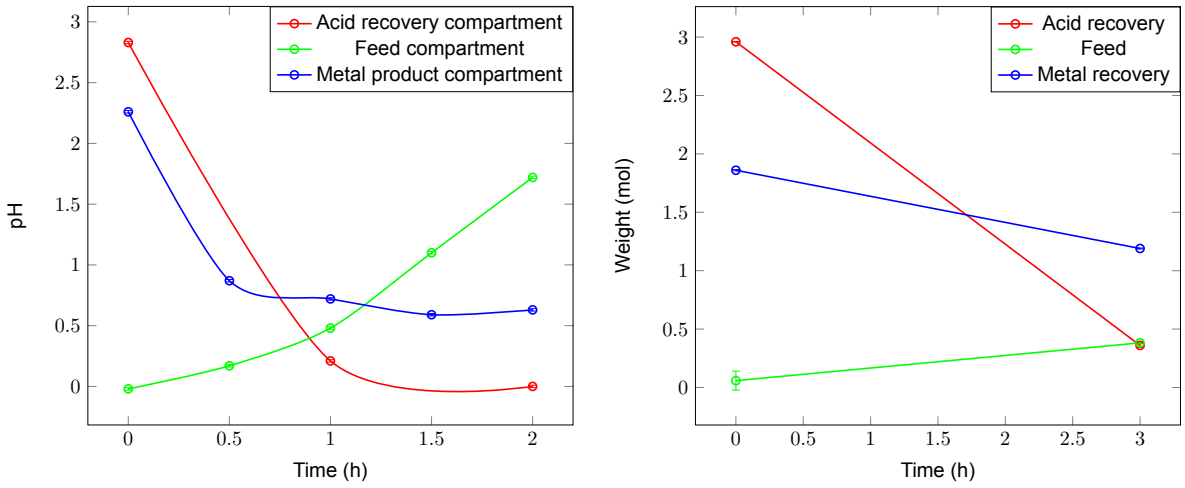

(a) Acidity of the electrolytic compartments during a constant voltage supply

(b) Acidity of the electrolytic compartments during the pulsating voltage supply

Figure 5.13: Acidity changes due to a pulsating voltage supply. The starting parameters for the experiments are displayed in table 5.17.

Figure 5.13a displays the acidity within the electrodialytic compartment during the constant voltage supply mode of operation, whilst figure 5.13b displays the results during the pulsating one. Interestingly,

the pulsating voltage supply seems to influence the acidity of the various compartments very strongly.

Referring to the Nernst-Planck relation shown in equation 5.2 a trivial prediction about how the pulsating flow should influence the acidity of the compartments can be made. Namely, since the voltage supply is turned on for half of the duration of the experiment when compared to the constant mode of operation, the proton transfer should decrease by a factor of 2. However, from figures 5.13a and refB it is made clear that the concentration of the proton transfer rate is influenced differently.

Let's take the metal product compartment pH of 0.6 at a time stamp of 1.5 hours in figure 5.13a, which equates to a proton concentration of 0.25 mol/L. According to our hypothesis, this pH should be matched at a timestamp of 3 hours in figure 5.13b. However, the recorded pH at this timestamps equals 1.2, which equates to a proton concentration of only 0.06 mol/L, a rough factor 5 lower than expected.

Whilst the true reason for this trend deserves further investigation, at this stage of the research it is simply noted that the pulsating voltage supply is not to be seen as an appropriate solution to the excessive gas generation issue.

Pulsating current influence on metal transfer rate
Under the previous header "Pulsating Current Influence on Acidity" a conclusion has been drawn about the ineffectiveness of the pulsating voltage supply as a method to solve the gas related problems. Nonetheless, an interesting observation can be made about the metal recovery effectiveness during this attempt, which is the main focus of this section.

Since the metal recovery results are a direct result of the experiment described in table 5.13, a repetition of the experimental procedure is eluded.

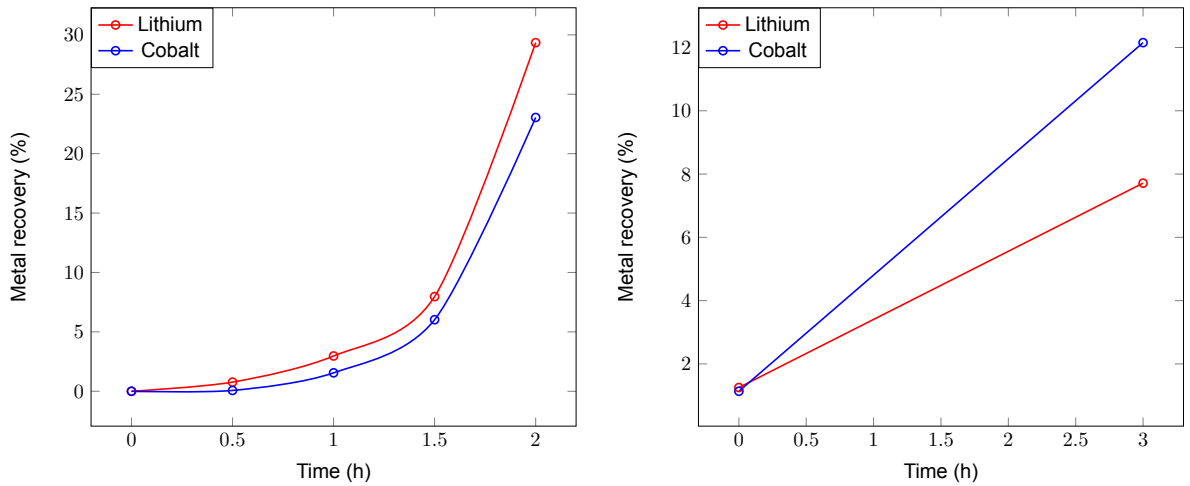

(a) Metal recovery at a constant voltage supply

(b) Metal recovery at a pulsating voltage supply

Figure 5.14: Metal recovery changes due to a pulsating voltage supply. The starting parameters for the experiments are displayed in table 5.17.

For convenience, figure 5.14a displays a copy of metal recovery efficiency shown earlier in figure 5.12b. Meanwhile, figure 5.14b displays the results for the pulsating voltage mode of operation. What is most interesting in these figures, is that the selectivity of the cobalt to lithium recovery seems to drastically change.

Whilst a definitive statement about the reason for this occurrence would require more investigation, an attempt at an educated guess can still be attempted. Namely, it is reasonable to assume that the back-diffusion rate of lithium ions from the metal product to the feed compartment is higher than the rate of the cobalt ions. This prediction is further supported by the results presented in figure 5.12, whereby

the selectivity changed significantly towards lithium as the applied voltage is decreased.

Projected Electrode Area Influence on Acidity
This section displays a second attempt at the resolution of gas related issues. In the attempt, the hydrogen and oxygen generation at the electrodes is lowered through a physical decrease of the effective electrode and membrane areas. In the context of BPMED, under a fixed voltage supply this change would cause the current density in the system to remain constant and the current itself to decrease, as displayed in figure 5.15.

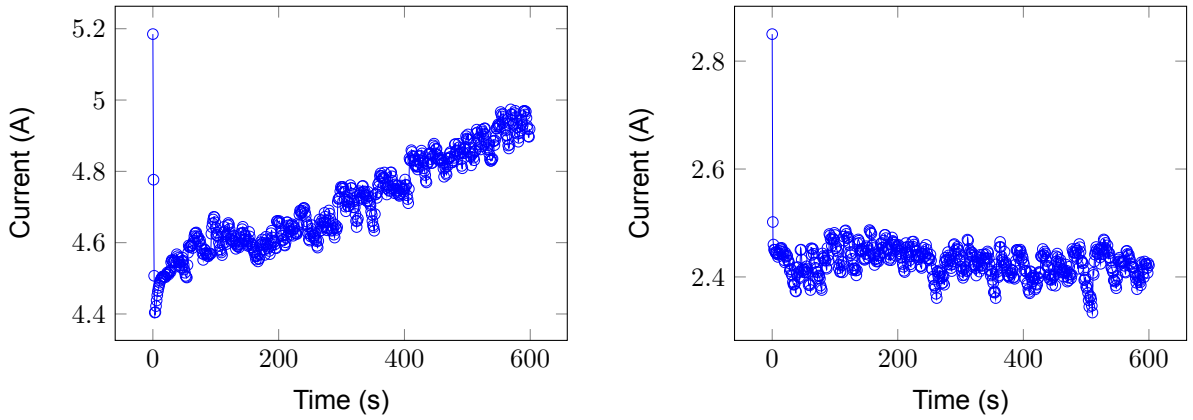

(a) Time-Current profile for an applied voltage of 12 V and a projected electrode area of 100 cm^2.

(b) Time-Current profile for an applied voltage of 12 V and a projected electrode area of 50 cm^2.

Figure 5.15: Time-Current profile for an applied voltage of 12 V and different projected electrode areas.

From figure 5.15b it is deduced that the average current density for a projected electrode area of 100 cm^2 and a supply voltage of 12 V is roughly 4.7 A per 100 cm^2, or 0.047 A/cm^2. Meanwhile, the current density for the same conditions, but a lower area in figure 5.15b is estimated to be 2.4 A per 50 cm^2, or 0.048 A/cm^2, which proves the previously established hypothesis.

Since this result, however, is in contradiction with the relationship between the projected area and current density in the context of electrolysis a small analysis of this statement is provided next.

To begin with, it is reasonable to assume that in the context of conventional electrolysis the determining factor for the maximum current at a particular voltage arises from the maximum rate at which ions can be supplied to the electrode. In the context of the BPMED setup, however, the current is most likely limited by the membrane's area resistance $\Omega\,cm^2$. A variable, that is often provided by manufacturer's in "Na^+ form", which implies that the resistance is conventionally provided for a 0.5 M NaCl solution at stp conditions. Therefore, if the membrane area is halved, so is the area resistance. Which, through Ohm's law, shown in equation 5.3, implies that the current is halved and the current density is unchanged.

$$V = I(\frac{S}{A}) \tag{5.3}$$

Whereby:

- J - current density
- A - membrane area
- A - area resistance

Ultimately, after prolonged operation of the stack in the reduced projected electrode area configuration it is concluded that the issues associated with the excessive gas generation has been solved. Thus, the focus in this section can be shifted from the feasibility of the solution to its effectiveness, which is seen as the motivation behind the experiments displayed next.

Starting parameters

The controlled parameters for the two trials are displayed below in table 5.18, whilst the independent parameter is shown in table 5.19. Crucially, it should be noted that the projected electrode area has physically been changed by covering the cutouts within all of the utilised gaskets in the BPMED setup with spare EPDM rubber in a manner that would minimize uneven current distribution.

Table 5.18: Controlled variables for the decreased area solution.

Controlled variable	Value
Applied voltage	12 V
Projected electrode area	100 cm^2
Flow rate in all compartments	48 ml/min
Starting composition of feed compartment	1M HNO_3, 1.7 %vol H_2O_2
Starting composition and volume of product compartment	300 ml of 0.5 M NaCl solution
Starting composition and volume of acid recovery compartment	300 ml of 0.5 M NaCl solution
Starting composition and volume of electrode rinse compartment	400 ml 0.5 M NaCl solution

Table 5.19: Independent variables for the decreased area solution.

Independent variable	Value in trial 1	Value in trial 2
Projected electrode area	100 cm^2	50 cm^2

Results

Figure 5.16a displays the outcome for the experiment conducted with a projected electrode area of 100 cm^2, whilst figure 5.16b the results for half of that area. Most importantly, the figure showcase that the acidity within the metal product compartment doesn't reach a pH below 1 once the area is halved, which significantly diminishes the potential the dissolution of cobalt ions.

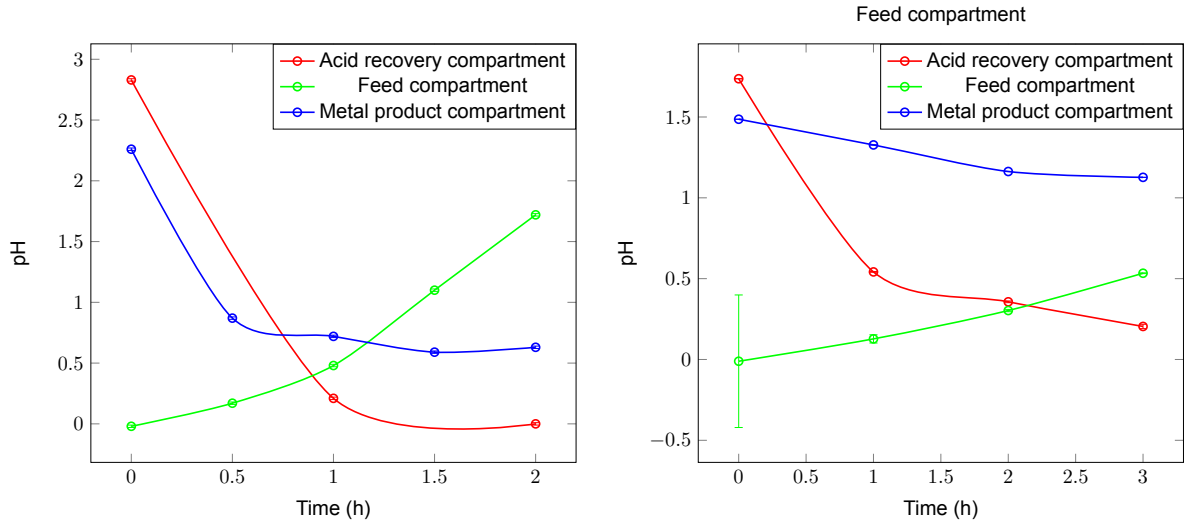

(a) Acidity of the electrolytic compartments at a projected electrode area of 100 cm^2.

(b) Acidity of the electrolytic compartments at a projected electrode area of 50 cm^2.

Figure 5.16: Acidity changes within the electrolytic compartments at different projected electrode areas. The experimental parameters for the experiments are displayed in tables 5.18 and 5.19.

In a first attempt to clarify the results, this research has noted that the proton and hydroxide production within the BPMs decreases with lower currents. This implies that in the metal product compartment

the supply of hydroxide ions from the BPM decreases, ultimately causing an increase in pH. However, this assumption is not observed from the results displayed in figure 5.16, but rather, the exact opposite effect is noted.

Whilst further investigation into the clarification of the results is required, this research postulates that the outcomes are a consequence of the fact that the diffusion rates due to Donnan Dialysis are significantly lower than the diffusion rates due to electroosmosis. A more elaborate description of this statement has been provided earlier in this section under the header “Volume Influence on Acidity”. In fact, it has been estimated that diffusion driven by electroosmosis is a factor 10 larger than the Donnan (diffusion) dialysis, which could potentially explain the observed trends.

5.4. Final Results and Implications

After the full resolution of issues associated with the initial design and subsequent optimization of experimental parameters, this section presents the most successful trial conducted in this research.

The section opens with an explanation of the chosen configuration and experimental parameters. Thereafter, it presents the experimental outcomes and clarifies their broader implications. Finally, the section states the overall conclusion for the research conducted in this report, providing answers to the research questions stated in the opening chapter and offers recommendations for future research.

Final configuration and operational parameters

Area

The final design configuration utilizes a reasonably small projected electrode area, as displayed in table 5.20. Whilst this relatively small area negatively impacts the rate of Donnan dialysis, it successfully manages to save the gaskets from failing due to excessive gas generation.

Flow rates

The effect of flow rates on the metal recovery efficiency was not investigated in this study due to time-constraints. Instead, this parameter has been held constant throughout the majority of this research in order to minimize its interference with the other system optimizations.

Applied Voltage

Due to the decrease in the projected electrode area for this experiment, the limit for the supply voltage is shifted upwards. Which, if utilized, would cause faster metal ion migration.

Nevertheless, in the final design configuration the voltage is kept at the 12 volts mark. The reason for this, is the fact that the acidity within the metal product compartment decreases at a reasonably slow rate. This results in the cobalt precipitating if the voltage supply is increased.

Starting composition of feed compartment

In order to increase the acidity of the metal product compartment solution during operation of the stack, the initial concentration of hydrogen ions within the feed compartment should be maximized. However, this optimization is limited by a pH stability bound for the cation exchange membrane, below which the membrane is expected to fail. Since this limit corresponds to a pH of 0, this acidity value is utilized within the feed compartment solution in the final optimization step.

The hydrogen peroxide concentration within the feed solution is set to 1.7 % vol. This is the minimum required value to ensure the reduction of the Co^{3+} ions to Co^{2+} ions within the leaching step. This, in turn, greatly improves the leaching efficiency.

Finally, the LCO concentration within the starting feed compartment solution is set to 3 grams per liter. Through the use of data, acquired in the course of this research, this concentration is calculated to lead to the maximum metal recovery.

Starting composition of acid recovery, metal product and the electrode rinse compartment solution

The starting solution for acid recovery and metal product compartments is set to constrain 0.5 M NaCl. Whilst higher concentration of NaCl within the metal product solution increases the Donnan dialysis effects, further optimization of this parameter has been eluded in lieu of time-constraints.

The starting electrode rinse compartment solution is set to contain 0.25 M Na_2SO_4. Importantly, the use of chlorine ions in this compartment has been avoided in order to prevent the potential generation of chlorine gas and subsequent damage to the BPMs.

Starting volumes

The starting volumes of the solutions utilized within the various electrodialytic compartments are minimized in order to lower the time required for the separation process to come to completion.

Table 5.20: Experimental parameters for the optimized design configuration.

Experimental parameters	Value
Projected electrode area	100 cm^2
Applied voltage	12 V
Flow rate in acid recovery, feed and metal product compartment	48 ml/min
Flow rate in electrode rinse compartment	100 ml/min
Starting composition of feed compartment	1M HNO_3, 1.7 %vol H_2O_2, 3 g/L LCO
Starting composition and volume of product compartment	300 ml of 0.5 M NaCl solution
Starting composition and volume of acid recovery compartment	300 ml of 0.5 M NaCl solution
Starting composition and volume of electrode rinse compartment	400 ml 0.25 M Na_2SO_4 solution

Final Results

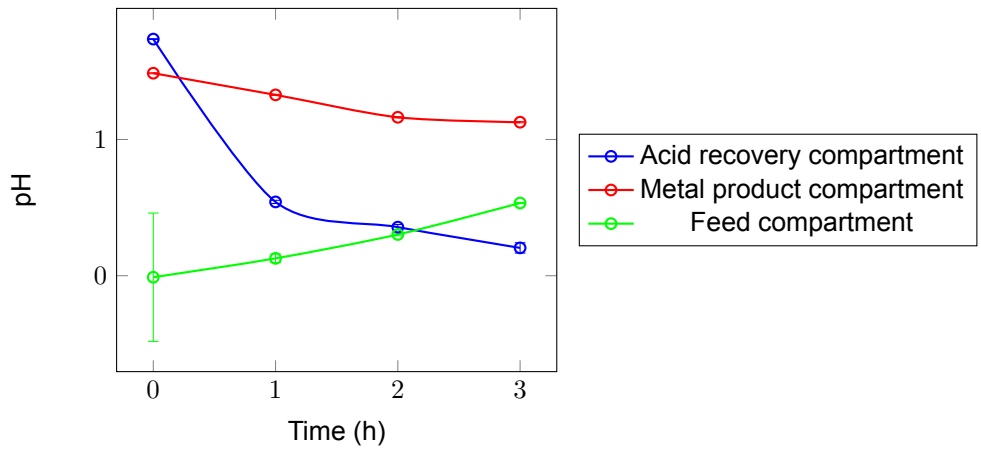

Figure 5.17: Acidity outcomes for the optimized design configuration. The experimental parameters of which are displayed in table 5.20.

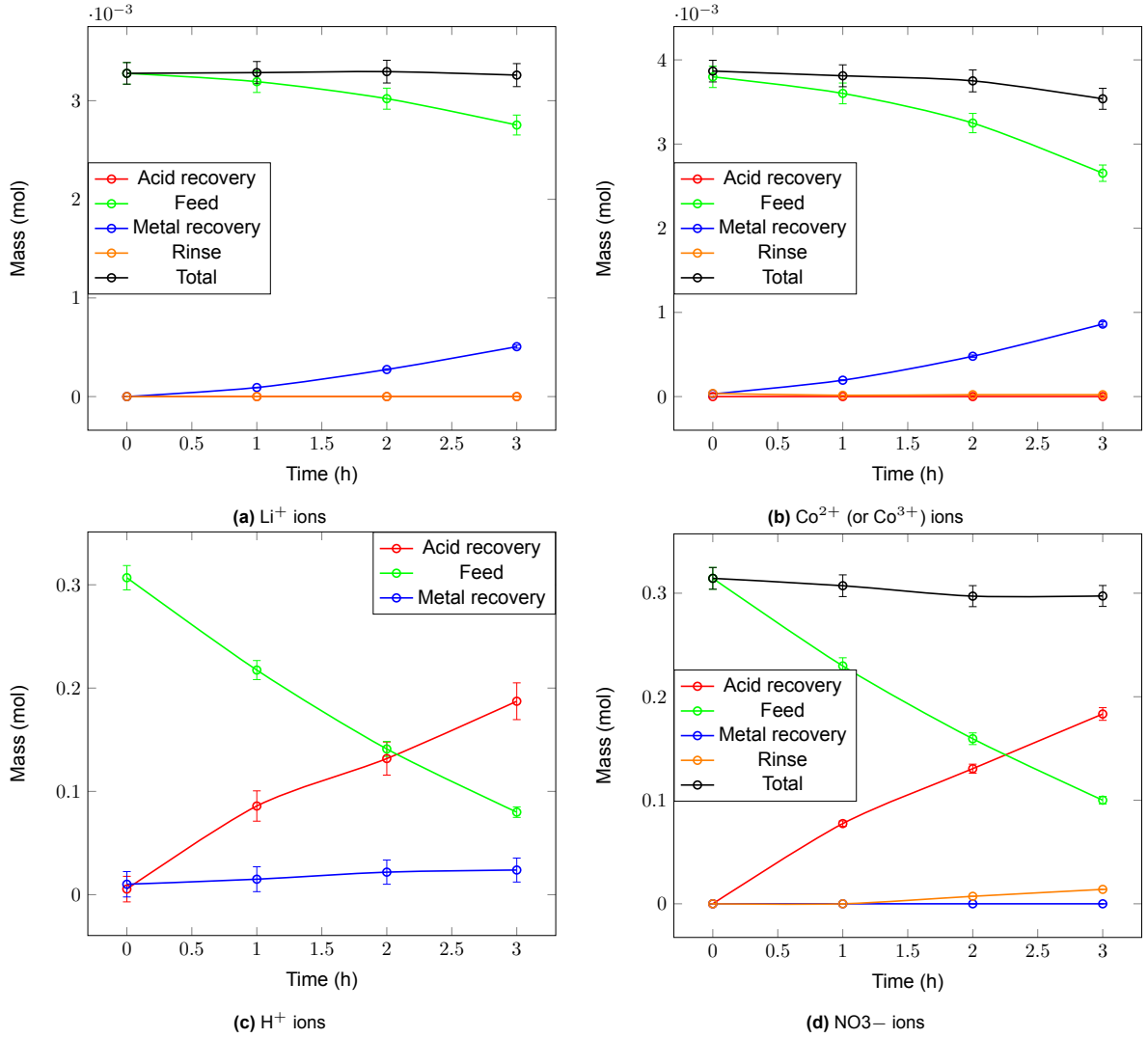

Figure 5.18: Recovery results for the optimized design configuration. The experimental parameters for this configuration are displayed in table 5.20.

The results for the optimized experimental parameters are displayed in figures 5.18, 5.17 and 5.19. Hereby, figure 5.17 showcases the acidity changes within the different compartments during operation, figure 5.18 the mass of the Li^+, Co^{2+} (or Co^{3+}), H^+ and $NO_3{}^-$ ions within the four electrolytic compartments and figure 5.19 the complete overview of the acquired data.

First and foremost, it is observed from figure 5.17 that the pH within the acid recovery compartment reaches a value of 0.2 at a timestamp of 3 hours. This acidity is higher than the initial acidity of the feed solution. However, from the works conducted by Lee and Rhee, it is postulated that no significant decrease in the leaching efficiency should be noticed if this acid was to be reused [44]. Next, figure 5.17 displays reasonably poor results for the pH decrease within the metal product compartment, as at the final timestamp of 3 hours it doesn't reach a value below 1.3.

Due to the poor transport of protons into the metal product compartment the oxidation of the Co^{2+} ion significantly increases, which hence lowers the solubility limit of the subsequently formed cobalt precipitate. This statement can be confirmed by the results displayed in figure 5.18b, which showcases a decrease in the total recorded cobalt mass.

Finally, the data in figures 5.18a and 5.18b can be used to derive that the cobalt and lithium recovery after three hours is 22 and 14 percent respectively. This provides the proof of concept for the BPMED

solution proposed in this report. Even though these recovery percentages seem inefficient, it is crucial to emphasize that these numbers are a direct consequence of the physical limitations of the setup utilized in this report, rather than the effectiveness of the concept as a whole.

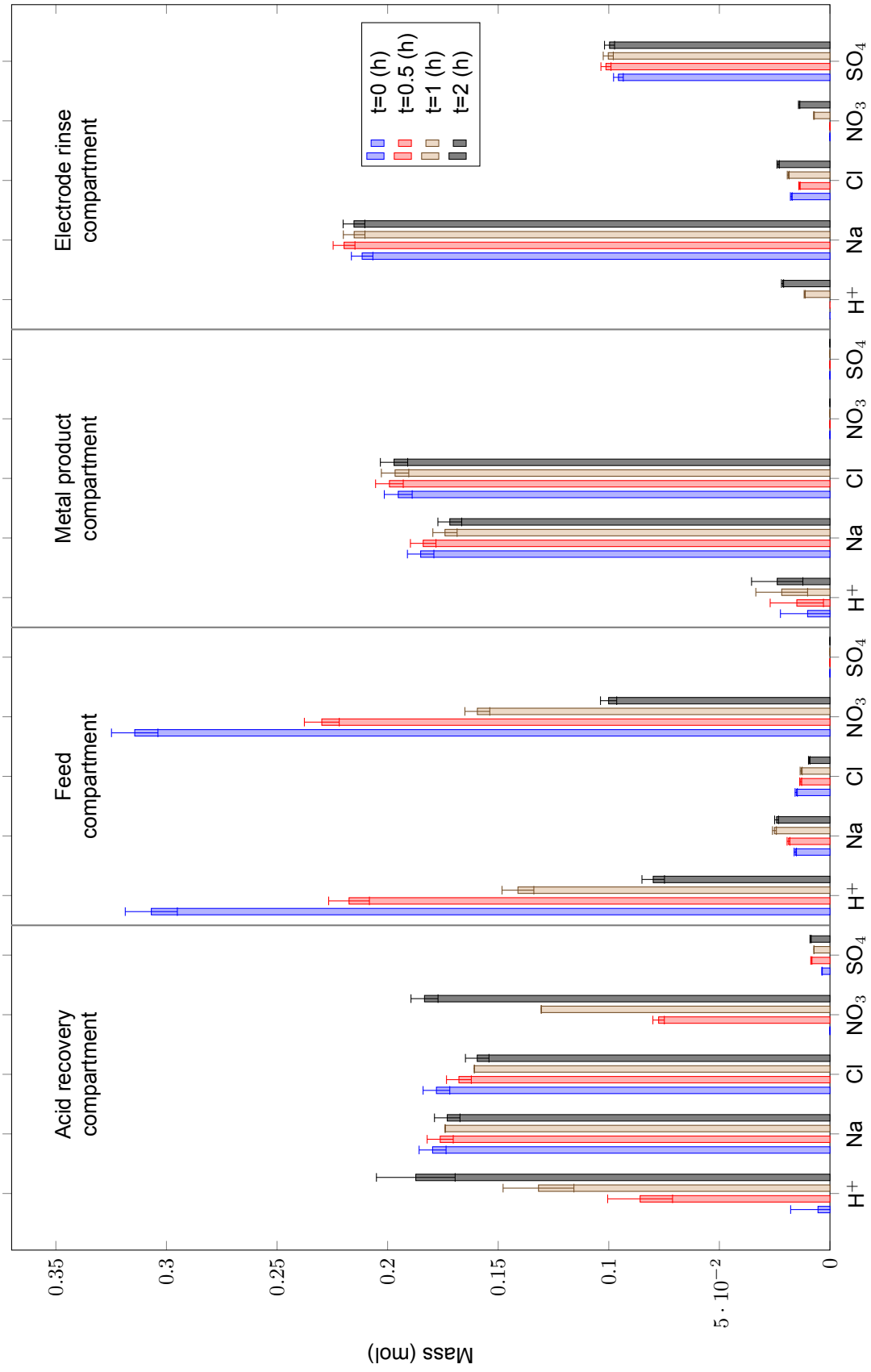

Figure 5.19: Full display of ions during the optimized design operation.

5.5. Conclusion and Recommendations

Conclusion
The main goal of the research presented in this report was to develop a working and scalable solution to the non-circular utilization of acids within the standard hydrometallurgical recycling route for LIBs. In order to achieve this objective, the study first investigated the advantages and drawbacks of state-of-the art electrochemical recycling methods within a literature review and proposed the use of BPMED in combination with Donnan (diffusion) dialysis as a means to minimize the shortcomings of this approach. Subsequently, the study postulated a research question and deconstructed it into three distinct sub questions in order to guide a targeted and structured development of the proposed solution.

In the next part of this research a working prototype of the BPMED setup was built, tested and optimized for the purpose of improved performance. In doing so, various troubleshooting methods were implemented in order to solve a number of engineering issues. Whilst most of the issues were physically resolved, other issues had proven to be inherent to flaws in the initial design and had to be bypassed by careful adjustments of the experimental parameters instead.

In this section, the overall implications of the optimized design and final results are showcased through an explicit answer to the study's main research question. In doing so, the answer is implicitly structured in a manner that closely resembles the layout proposed by the three established subquestions. Finally, the report illuminates the shortcomings of the conducted research and concludes with a number of recommendations for future research.

How to utilize bipolar membrane electrodialysis as a tool to recover lithium and cobalt from leached LCO cathode material?

To the best of our knowledge, BPMED is the only electrochemical solution that allows for simultaneous regeneration of lithium, cobalt, as well as the leaching agent from leached LCO cathode material in a fully closed-loop manner. Meaning, that the use of this technology, contrary to its alternatives, does not entail the consummation of additional material in order to effectively separate the valuable components from its unnecessary constituents. Therefore, for a well-constructed development of the answer to the research question it is crucial that the BPMED system be designed in a manner that maximises this particular advantage.

Throughout the experimental phase of this research a number of key challenges, inherent to the proposed solution, have been identified. The effectiveness of the solutions to these challenges, subsequently determines the overall effectiveness of BPMED setup as a means to recover valuable material from spent LIBs as a whole.

One such challenge, identified early in the experimental process, is the tendency of the Co^{2+} ions to oxidise within the metal recovery compartment and precipitate in the form of cobalt oxide. If left untreated, this precipitation could eventually block exits and entrances to the flow chambers, create uneven current distributions or break the diaphragm pumps utilized in the setup.

After careful investigation of the conditions aimed at increasing the solubility limit of cobalt oxide, this research postulates the following statement: the only feasible solution to the precipitation issue that simultaneously adheres to the closed-loop recovery objective, is the incorporation of Donnan (diffusion) dialysis into the existing BPMED configuration. In doing so, protons from the feed compartment interchange with sodium ions from the metal recovery compartment, effectively decreasing the pH of its respective solution.

Unfortunately, an accurate representation of the solution's effectiveness was hindered by limitations of the experimental setup. As confirmed by both theory and experimental results, in order for the Donnan dialysis effects to be noticeable within the timeframe of a single experiment, the effective membrane areas need to be increased beyond the capacity of the flow chambers. That is, if the Donnan dialysis and the electro-osmosis are to be used simultaneously, rather than in sequence.

Nevertheless, whilst this research fails to provide an accurate representation of the potential metal recovery efficiency that can be achieved through the integration of Donnan dialysis into BPMED, the study successfully establishes a robust proof of concept. To be precise, within a timeframe of three hours, the setup effectively lowers pH within the metal product recovery from neutral to 1.2, and manages to respectively recover 14 and 22 percent of the lithium and cobalt initially present in the feed solution. Furthermore, throughout the entire course of this research the BPMED setup has consistently proven to successfully recover the leaching acid, easily reaching concentrations of around 0.6 M.

Having said that, this research underlines that the absolute amount of material that can be recovered through the optimized setup is very low when compared to the absolute amount of required leaching agent. Whilst this setup can be used to recover trace amounts of metal, as well as the leaching agent, the scalability of this design leaves room for improvement. Consequently, in order to increase the scalability potential additional optimization steps are required.

First and foremost, the membrane area needs to be increased in order to promote Donnan dialysis. Secondly, the starting LCO concentration in the feed compartment must be tailored to the solubility limit of the metal within the product compartment. Finally, it has been observed that the supply voltage has a significant effect on the selectivity of the CEM and thus requires optimization.

Recommendations

The research conducted in this study led to the successful incorporation of Donnan dialysis into a BPMED setup. In doing so, a viable solution to the excessive acid usage within the hydrometallurgical recycling approach was demonstrated. The operational parameters utilized in this proof, however, were not optimized to a level, whereby a techno-economic analysis of the BPMED setup would be appropriate. Therefore, the study emphasizes that the conducted research contains a variety of areas for improvement, which are summarized in this final section of the report.

1. Over the course of this research, the performance of the setup was optimized to a certain extent. However, the effectiveness of this optimization was significantly hindered by the physical dimensions of the stack. Firstly, as a result of the stack's large parameters the experiments required a significant amount of reactants, all of which needed the appropriate time for preparation and disposal. Secondly, the stack was hard to fill and empty, as significant time and effort was required to operate it. Therefore, in order to simplify the investigation into the relationship between certain operational parameters and the experimental outcomes, it is advised that a smaller cell be purchased or made.
2. This research proved that BPMED can be used to recycle metal material from pure cathode material. However, industrially leached LIB material is expected to contain a number of impurities, the effect of which remains to be investigated. In all likelihood, the operational parameters of the BPMED system would have to be adjusted in order to minimize the effects of the impurities. Additionally, a more rigorous pre- and post treatment of the LIBs would be required.
3. In future research it is advised that the recovered leaching agent be reused in the experiments. This quantifies the extent to which the purity and concentration of the recovered acid remains stable. The process is especially relevant in case the conducted experiments permit the added contamination of impurities into the feed solution.

Over the course of this research it was postulated that the precipitation of metal material in the BPMED system would cause detrimental problems. Whilst this holds true for the design utilized in this study, it is crucial to emphasize that alternative systems could be developed in order to support precipitation.

At this stage, it is not possible to preemptively determine whether such a system would turn out to be more efficient than the one developed in this research. In most industrial systems precipitation is avoided in order to minimize ohmic losses, fouling and other issues. Nonetheless, this research

showed that the requirement for the complete dissolution of metal material creates its own issues. Subsequently, this study recommends that a different system, built specifically for the purpose of precipitation, be developed in parallel to the one presented in this report. In an attempt to guide the successful development hereof, the following recommendations are given.

1. The precipitated material should not be circulated within the alternative design. Rather, an engineering solution should be developed outside of the stack in order to effectively remove solid material from the loop that connects the system's output to its input. Some type of quick filtration process could be utilized for this aim, whereby the emphasis is laid upon the filtration's rate, rather than its efficiency.
2. It is advised that the electrolytic flow chambers, as well as the utilized tubing be widened in order to prevent clogging.
3. The alternative design should not contain zones, which encourage the accumulation of precipitate material. Especially within the stack itself, the use of sharp edges or corners should be avoided. Additionally, this research recommends that the electrolytic solutions within the stack be pumped from top to bottom, in order to reduce the force required to remove the solid material from the setup.

Bibliography

[1] Bin Huang et al. “Recycling of lithium-ion batteries: Recent advances and perspectives”. In: *Journal of Power Sources* 399 (Sept. 2018), pp. 274–286. ISSN: 03787753. DOI: 10.1016/j.jpowsour.2018.07.116.

[2] Liu Yun et al. “Metallurgical and mechanical methods for recycling of lithium-ion battery pack for electric vehicles”. In: *Resources, Conservation and Recycling* 136 (Sept. 2018), pp. 198–208. ISSN: 0921-3449. DOI: 10.1016/j.resconrec.2018.04.025.

[3] Colin McKerracher et al. *EVO Report 2023*. URL: https://about.bnef.com/electric-vehicle-outlook/.

[4] Naoki Nitta et al. “Li-ion battery materials: present and future”. In: *Materials Today* 18.5 (June 2015), pp. 252–264. ISSN: 1369-7021. DOI: 10.1016/j.mattod.2014.10.040.

[5] Brian Makuza et al. “Pyrometallurgical options for recycling spent lithium-ion batteries: A comprehensive review”. In: *Journal of Power Sources* 491 (Apr. 2021). ISSN: 0378-7753. DOI: 10.1016/j.jpowsour.2021.229622.

[6] Donald E. Garrett. *Handbook of Lithium and Natural Calcium Chloride*. Elsevier, Apr. 2004. ISBN: 978-0-08-047290-4.

[7] Beatriz Bustos-Gallardo, Gavin Bridge, and Manuel Prieto. “Harvesting Lithium: water, brine and the industrial dynamics of production in the Salar de Atacama”. In: *Geoforum* 119 (Feb. 2021), pp. 177–189. ISSN: 0016-7185. DOI: 10.1016/j.geoforum.2021.01.001.

[8] Amato Alessia et al. “Challenges for sustainable lithium supply: A critical review”. In: *Journal of Cleaner Production* 300 (June 2021). ISSN: 09596526. DOI: 10.1016/j.jclepro.2021.126954.

[9] Shahjadi Hisan Farjana, Nazmul Huda, and M. A. Parvez Mahmud. “Life cycle assessment of cobalt extraction process”. In: *Journal of Sustainable Mining* 18.3 (Aug. 2019), pp. 150–161. ISSN: 2300-3960. DOI: 10.1016/j.jsm.2019.03.002.

[10] F. K. Crundwell, N. B. du Preez, and B. D. H. Knights. “Production of cobalt from copper-cobalt ores on the African Copperbelt – An overview”. In: *Minerals Engineering* 156 (Sept. 2020). ISSN: 0892-6875. DOI: 10.1016/j.mineng.2020.106450.

[11] United Nations. *Resolution 2717*. Dec. 2023. URL: https://monusco.unmissions.org/en/resolution-2717-2023.

[12] Dana Thompson et al. “To shred or not to shred: A comparative techno-economic assessment of lithium ion battery hydrometallurgical recycling retaining value and improving circularity in LIB supply chains”. In: *Resources, Conservation and Recycling* 175 (Dec. 2021). ISSN: 0921-3449. DOI: 10.1016/j.resconrec.2021.105741.

[13] European Commission. *Proposal for a regulation of the European Parliament and of the Council concerning batteries and waste batteries, repealing Directive 2006/66/EC and amending Regulation (EU) No 2019/1020*. en. Oct. 2020. URL: https://eur-lex.europa.eu/legal-content/EN/TXT/DOC/?uri=CELEX:52020PC0798.

[14] Joey Chung-Yen Jung, Pang-Chieh Sui, and Jiujun Zhang. “A review of recycling spent lithium-ion battery cathode materials using hydrometallurgical treatments”. In: *Journal of Energy Storage* 35 (Mar. 2021), p. 102217. ISSN: 2352-152X. DOI: 10.1016/j.est.2020.102217. URL: https://www.sciencedirect.com/science/article/pii/S2352152X20320405.

[15] Yi Ji et al. “Direct recycling technologies of cathode in spent lithium-ion batteries”. In: *Clean Technologies and Recycling* 1.2 (2021), pp. 124–151. ISSN: 2770-4580. DOI: 10.3934/ctr.2021007.

[16] Zhengming John Zhang and Premanand Ramadass. “Lithium-Ion Battery Systems and Technology”. In: *Batteries for Sustainability: Selected Entries from the Encyclopedia of Sustainability Science and Technology*. Springer, 2013, pp. 319–357. DOI: 10.1007/978-1-4614-5791-6_10.

[17] T. Li et al. “Degradation Mechanisms and Mitigation Strategies of Nickel-Rich NMC-Based Lithium-Ion Batteries”. In: *Electrochemical Energy Reviews* 3.1 (2020), pp. 43–80. DOI: 10.1007/s41918-019-00053-3.

[18] Jing Li et al. “Study of the Failure Mechanisms of LiNi0.8Mn0.1Co0.1O2 Cathode Material for Lithium Ion Batteries”. en. In: *Journal of The Electrochemical Society* 162.7 (Apr. 2015). ISSN: 1945-7111. DOI: 10.1149/2.1011507jes.

[19] M. M. Cerrillo-Gonzalez et al. “Recovery of Li and Co from LiCoO2 via Hydrometallurgical–Electrodialytic Treatment”. In: *Applied Sciences* 10.7 (Jan. 2020). ISSN: 2076-3417. DOI: 10.3390/app10072367.

[20] Zhilin Liang et al. “Hydrometallurgical Recovery of Spent Lithium Ion Batteries: Environmental Strategies and Sustainability Evaluation”. In: *ACS Sustainable Chemistry & Engineering* 9.17 (May 2021). DOI: 10.1021/acssuschemeng.1c00942.

[21] Zachary J. Baum et al. “Lithium-Ion Battery Recycling–Overview of Techniques and Trends”. In: *ACS Energy Letters* 7.2 (Feb. 2022), pp. 712–719. DOI: 10.1021/acsenergylett.1c02602.

[22] Mengyuan Chen et al. “Recycling End-of-Life Electric Vehicle Lithium-Ion Batteries”. In: *Joule* 3.11 (Nov. 2019). ISSN: 2542-4785, 2542-4351. DOI: 10.1016/j.joule.2019.09.014.

[23] Huayi Yin and Pengfei Xing. “Pyrometallurgical Routes for the Recycling of Spent Lithium-Ion Batteries”. In: *Recycling of Spent Lithium-Ion Batteries: Processing Methods and Environmental Impacts*. 2019, pp. 57–83. ISBN: 978-3-030-31834-5. DOI: 10.1007/978-3-030-31834-5_3.

[24] Reiner Sojka. *Accurec invests and signs long term contracts*. Nov. 2017. URL: https://accurec.de/accurec-invests-and-signs-long-term-contracts?lang=en.

[25] Mohammad Assefi et al. “Pyrometallurgical recycling of Li-ion, Ni–Cd and Ni–MH batteries: A minireview”. In: *Current Opinion in Green and Sustainable Chemistry* 24 (Aug. 2020), pp. 26–31. ISSN: 2452-2236. DOI: 10.1016/j.cogsc.2020.01.005.

[26] Yiqi Tang et al. “Recovery and regeneration of LiCoO2-based spent lithium-ion batteries by a carbothermic reduction vacuum pyrolysis approach: Controlling the recovery of CoO or Co”. In: *Waste Management* 97 (Sept. 2019), pp. 140–148. ISSN: 0956-053X. DOI: 10.1016/j.wasman.2019.08.004.

[27] Alexandre Chagnes and Jolanta Swiatowska. *Lithium Process Chemistry: Resources, Extraction, Batteries, and Recycling*. Elsevier, June 2015.

[28] Liang Sun and Keqiang Qiu. “Vacuum pyrolysis and hydrometallurgical process for the recovery of valuable metals from spent lithium-ion batteries”. In: *Journal of Hazardous Materials* 194 (Oct. 2011), pp. 378–384. ISSN: 0304-3894. DOI: 10.1016/j.jhazmat.2011.07.114.

[29] Fabian Diaz et al. “Degradation Mechanism of Nickel-Cobalt-Aluminum (NCA) Cathode Material from Spent Lithium-Ion Batteries in Microwave-Assisted Pyrolysis”. In: *Metals* 8.8 (Aug. 2018), p. 565. ISSN: 2075-4701. DOI: 10.3390/met8080565.

[30] Swapan Kumar Haldar. “Chapter 13 - Mineral Processing”. In: *Mineral Exploration (Second Edition)*. Elsevier, Jan. 2018, pp. 259–290. ISBN: 978-0-12-814022-2. DOI: 10.1016/B978-0-12-814022-2.00013-7.

[31] Linda Reinhart et al. “Pyrometallurgical recycling of different lithium-ion battery cell systems: Economic and technical analysis”. In: *Journal of Cleaner Production* 416 (Sept. 2023). ISSN: 0959-6526. DOI: 10.1016/j.jclepro.2023.137834.

[32] Tairan Yang et al. “An Effective Relithiation Process for Recycling Lithium - Ion Battery Cathode Materials”. In: *Advanced Sustainable Systems* 4 (Dec. 2019). DOI: 10.1002/adsu.201900088.

[33] Jennifer B. Dunn et al. *Material and Energy Flows in the Materials Production, Assembly, and End-of-Life Stages of the Automotive Lithium-Ion Battery Life Cycle*. Technical Report ANL/ESD/12-3 Rev. Argonne National Lab. (ANL), Jan. 2014. DOI: 10.2172/1177517.

[34] Rebecca E. Ciez and J. F. Whitacre. “Examining different recycling processes for lithium-ion batteries”. In: *Nature Sustainability* 2.2 (Feb. 2019). Publisher: Nature Publishing Group, pp. 148–156. ISSN: 2398-9629. DOI: 10.1038/s41893-019-0222-5.

[35] David da Silva Vasconcelos et al. “Circular Recycling Strategies for LFP Batteries: A Review Focusing on Hydrometallurgy Sustainable Processing”. In: *Metals* 13.3 (Mar. 2023). Number: 3 Publisher: Multidisciplinary Digital Publishing Institute, p. 543. ISSN: 2075-4701. DOI: 10.3390/met13030543.

[36] Gavin Harper et al. “Recycling lithium-ion batteries from electric vehicles”. In: *Nature* 575.7781 (Nov. 2019), pp. 75–86. ISSN: 1476-4687. DOI: 10.1038/s41586-019-1682-5.

[37] Tao Zhang et al. “Chemical and process mineralogical characterizations of spent lithium-ion batteries: An approach by multi-analytical techniques”. In: *Waste Management* 34.6 (June 2014). ISSN: 0956-053X. DOI: 10.1016/j.wasman.2014.01.002.

[38] Seung-Hwan Lee, Hyun-Soo Kim, and Bong-Soo Jin. “Recycling of Ni-rich Li(Ni0.8Co0.1Mn0.1)O2 cathode materials by a thermomechanical method”. In: *Journal of Alloys and Compounds* 803 (Sept. 2019). ISSN: 0925-8388. DOI: 10.1016/j.jallcom.2019.06.229.

[39] Zheng Li et al. “Recovery of Lithium and Manganese from Scrap LiMn2O4 by Slurry Electrolysis”. In: *ACS Sustainable Chemistry & Engineering* 7.19 (Oct. 2019). DOI: 10.1021/acssuschemeng.9b04127.

[40] Alexandru Cătălin Sonoc et al. “A study of the application of Donnan dialysis to the recycling of lithium ion batteries”. In: *Hydrometallurgy* 175 (Jan. 2018), pp. 133–143. ISSN: 0304-386X. DOI: 10.1016/j.hydromet.2017.10.004.

[41] Alexandru C. Sonoc and Jack Jeswiet. “Application of Donnan Dialysis to the Separation and Recovery of Cations During Hydrometallurgical Recycling of Lithium Ion Batteries”. en. In: *Extraction 2018*. Ed. by Boyd R. Davis et al. Cham: Springer International Publishing, 2018, pp. 1855–1866. ISBN: 978-3-319-95022-8. DOI: 10.1007/978-3-319-95022-8_154.

[42] Ka Ho Chan, Monu Malik, and Gisele Azimi. “Separation of lithium, nickel, manganese, and cobalt from waste lithium-ion batteries using electrodialysis”. In: *Resources, Conservation and Recycling* 178 (Mar. 2022), p. 106076. ISSN: 0921-3449. DOI: 10.1016/j.resconrec.2021.106076.

[43] Atsushi Iizuka et al. “Separation of lithium and cobalt from waste lithium-ion batteries via bipolar membrane electrodialysis coupled with chelation”. In: *Separation and Purification Technology* 113 (July 2013), pp. 33–41. ISSN: 1383-5866. DOI: 10.1016/j.seppur.2013.04.014.

[44] Churl Kyoung Lee and Kang-In Rhee. “Preparation of LiCoO2 from spent lithium-ion batteries”. In: *Journal of Power Sources* 109.1 (June 2002), pp. 17–21. ISSN: 0378-7753. DOI: 10.1016/S0378-7753(02)00037-X.

[45] F. G Wilhelm et al. “Optimisation strategies for the preparation of bipolar membranes with reduced salt ion leakage in acid–base electrodialysis”. In: *Journal of Membrane Science* 182.1 (Feb. 2001), pp. 13–28. ISSN: 0376-7388. DOI: 10.1016/S0376-7388(00)00519-6.

[46] Eliana Guadalupe Pinna et al. “Acid leaching of licoo2 from libs: thermodynamic study and reducing agent effect”. In: (Apr. 2019). ISSN: 1665-2738.

[47] Karl H. Gayer and Arthur B. Garrett. “The Solubility of Cobalt Hydroxide, Co(OH)2, in Solutions of Hydrochloric Acid and Sodium Hydroxide at 25°”. In: *Journal of the American Chemical Society* 72.10 (1950), pp. 4032–4034. DOI: 10.1021/ja01164a019.

[48] A. D. MacGillivray. “Nernst Planck Equations and the Electroneutrality and Donnan Equilibrium Assumptions”. In: *The Journal of Chemical Physics* 48.7 (Apr. 1968), pp. 2903–2907. ISSN: 0021-9606. DOI: 10.1063/1.1669549.

A

Final Run Data

Acid Recovery Compartment								Feed Compartment							
		Ion concentration (PPM)								Ion concentration (PPM)					
Time (h)	Volume (mL)	Li	Co	Na	Cl	NO3	SO4	Time (h)	Volume (mL)	Li	Co	Na	Cl	NO3	SO4
-	300	0	0	14195	22608	0	0	-	300	83	0	0	0	73220	0
0	294.8675	0	0	14008	21391	0	1164	0	299.2675	76	748	1205	1808	65131	0
1	298.7675	0	0	13560	19906	16079	2704	1	291.5675	76	728	1478	1608	48862	0
2	299.5675	0	0	13351	19026	27015	2317	2	283.2675	74	676	2038	1631	34898	0
3	299.7675	0	0	13271	18861	37920	2803	3	272.9675	70	573	2033	1217	22735	0
Metal Product Compartment								**Electrode Rinse Compartment**							
		Ion concentration (PPM)								Ion concentration (PPM)					
Time (h)	Volume (mL)	Li	Co	Na	Cl	NO3	SO4	Time (h)	Volume (mL)	Li	Co	Na	Cl	NO3	SO4
-	300	0	0	14195	22608	0	0	-	500	0	0	11109	0	0	21897
0	309.4675	0	6	13748	22360	0	0	0	435.4675	0	5	11167	1423	0	21099
1	318.2675	2	36	13285	22186	0	0	1	445.1675	0	2	11346	1097	0	21854
2	317.2675	6	89	12613	21970	0	0	2	440.2675	0	3	11234	1520	1018	21870
3	319.2675	11	159	12377	21885	0	0	3	438.4675	0	3	11284	1895	1970	21833

B

Python Code for Pusation Frequency

```python
import numpy as np
import matplotlib.pyplot as plt
from scipy.interpolate import interp1d

I = np.linspace(0,10,31)

th = 1* (10**-1) #cm comp
Vol_comp = 10*10*th
Av = 6 * (10**23) # avogardos number
L = 22.4 # Liters/mol
e = 1.6 * (10**-19) #coulombs

c = np.zeros(len(I))
d = np.zeros(len(I))
mL_per_s_needed = np.zeros(len(I))
for i in range(len(I)):
    a = I[i] / e #electrons/s
    b = a/2 #Hydrogen atoms/s
    c[i] = b / Av #Hydrogen mols/s
    d[i] = (c[i] * L) * 1000 #hydrogen ml/s at different currents
    print(d[i])


# Let's assume that I can take away 30 ml/s, because my pumps doesn't seem
# to be working properly.
V_take_away = 50 # ml/min
V_take_away = V_take_away/60 #mL/s

time = np.linspace(0,20,21)
Bub_prod = np.zeros(len(time))

def function1(blub):
    for i in range(len(Bub_prod)):
        Bub_prod[i] = time[i]*blub


    Take_away = np.zeros(len(time))
    for i in range(len(Take_away)):
        Take_away[i]= V_take_away* time[i]


    # How many bubbles are inside stack
    bubbles_in_stack = np.zeros(len(time))
    for i in range(len(time)):
        bubbles_in_stack[i] = Bub_prod[i] - Take_away[i]

    plt.figure(1)
    plt.plot(time,Bub_prod, color = 'b')
    plt.plot(time, Take_away, color = 'g')
    plt.plot(time, bubbles_in_stack, color = 'k')
```

```
    plt.axhline(y=10, color='r', linestyle='--', label='Vertical Line')
    plt.show()

    interpolation_func = interp1d(bubbles_in_stack,time, bounds_error=False, fill_value="
        extrapolate")

    # Find x when y is 0.5
    desired_y = 10 #ml
    x_value = interpolation_func(desired_y)

    return x_value

for i in range(len(I)):
    function1(d[i])
    print(function1(d[i]), 'at', I[i], 'A', '=Time required to break gaskets')

print(10/V_take_away, 'time required to fix stack')
```

C

Nova Script for Optimized Setup

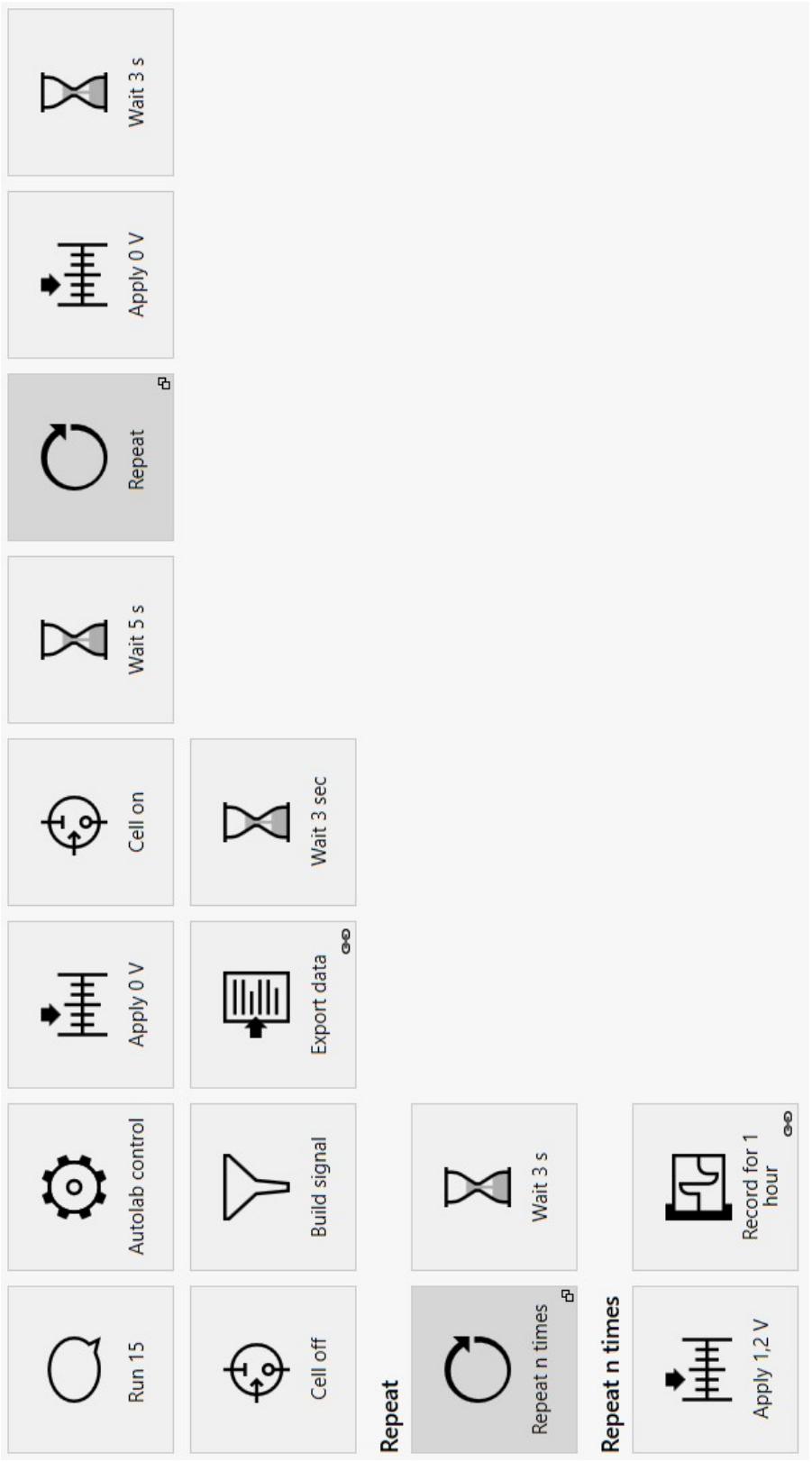
Run 15
Autolab control
Apply 0 V
Cell on
Wait 5 s
Repeat
Apply 0 V
Wait 3 s
Cell off
Build signal
Export data
Wait 3 sec
Repeat
Repeat n times
Wait 3 s
Repeat n times
Apply 1,2 V
Record for 1 hour

D

ElectroMP Cell Data

Electrical Data	
Projected electrode area, min [m²]	0.01
Projected electrode area, max [m²]	0.2
Current density, max [kA/m²]	4
Electrode gap range [mm]	2-16
Standard electrode gap [mm]	8
Stack Dimensions	
Height [mm]	306
Width [mm]	182
Length [mm]	>38
Pipe Connections	
Connections	Female ½” NPT
Electrolyte Flow Data	
Number of flow compartments	4
Max electrolyte flow per module	20-80
Electrolyte flow per frame	1-4
Frame width	100 [mm]
Frame height	100 [mm]
Frame thickness	10[mm]
Mesh parameters	0.25 x 0.25 [mm x mm]
Flow in each cell [m/s]	0.5-50
Materials	
Flow frame materials	PP
Gasket material	EPDM
Electrode material	Pt on Ti